1 **Structural and functional leaf diversity lead to variability in photosynthetic capacity across**

2 **a range of *Juglans regia* genotypes**

3

4

5 Mina Momayyezi[1*], Devin A. Rippner[2], Fiona V. Duong[1], Pranav V. Raja[1], Patrick J. Brown[3],

6 Daniel A. Kluepfel[4], J. Mason Earles[1], Elisabeth J. Forrestel[1], Matthew E. Gilbert[3], and Andrew

7 J. McElrone[1,4*]

8

9 [1]Department of Viticulture and Enology, University of California, Davis, California 95616 USA

10 [2]USDA-ARS, Horticultural Crops Research Unit, Prosser WA, 99350 USA

11 [3]Department of Plant Sciences, University of California, Davis, California 95616 USA

12 [4]USDA-ARS, Crops Pathology and Genetics Research Unit, Davis, CA, 95616 USA

13

14

15

16 *Corresponding authors: andrew.mcelrone@usda.gov; mmomayyezi@ucdavis.edu

17

18 **Summary Statement:**

19 *Juglans regia* accessions originating from lower latitudes exhibited enhanced photosynthetic

20 capacity associated with increased gas-phase diffusion, and leaf nitrogen, and lower leaf mass and

21 stomatal density. These accessions hold potential to improve productivity and stress tolerance for

22 commercial production.

23

24

25

26

Abstract

Similar to other cropping systems, few walnut cultivars are used as scion in commercial production. Germplasm collections can be used to diversify cultivar options and hold potential for improving crop productivity, disease resistance and stress tolerance. In this study we explored the anatomical and biochemical bases of photosynthetic capacity in 11 *J. regia* accessions in the USDA-ARS National Clonal Germplasm Repository. Net assimilation rate (A_n) differed significantly among accessions and was greater in those from lower latitudes coincident with increases in stomatal and mesophyll conductance, leaf thickness, mesophyll porosity and gas-phase diffusion, and leaf nitrogen, and lower leaf mass and stomatal density. High CO_2-saturated assimilation rates led to increases in A_n under limiting conditions. Greater A_n was found in lower latitude accessions native to climates with more frost-free days, greater precipitation seasonality, and lower temperature seasonality. As expected, water stress consistently impaired photosynthesis with the highest % reductions in three lower latitude accessions (A3, A5, and A9), which had the highest A_n under well-watered conditions. However, A_n for A3 and A5 remained amongst the highest under dehydration. *J. regia* accessions, which have leaf structural traits and biochemistry that enhance photosynthesis, could be used as commercial scions or breeding parents to enhance productivity.

Keywords: Photosynthetic capacity, *Juglans regia*, wild accessions, leaf anatomy, CO_2 conductance

Introduction

Common walnut, *Juglans regia* L., is an important and widely-grown agronomic species with major production areas concentrated in the northern hemisphere. Its natural range encompasses mountains from western China to central Asia (McGranahan & Leslie, 2009), and was extended by humans spreading the species throughout eastern and southwestern Europe from Central Asia (Leslie & McGranahan, 1998). Throughout its natural habitat, *J. regia* grows under a range of climatic conditions with mean monthly maximum temperatures ranging from -9 to +30˚C and annual cumulative precipitation from 175 to 1150 mm during the growing season (Geospatial Data, FAO 2021; Duke, 1978) (Supporting Information, Fig. S1). *J. regia* has been utilized to develop commercial scion cultivars (e.g. Chandler) and hybrid rootstocks with resistance to abiotic and biotic stresses (Leslie, *et al.* 2015; Kluepfel *et al.* 2015). Global walnut production is highly dependent on the limited genetic diversity of the commonly used scions. For example, only four scion cultivars account for ~ 80% of total yields. This results in orchard susceptibility to abiotic stresses, disease and pathogens. In California, the Chandler cultivar accounts for 50% of productive acreage (USDA-NASS 2020), but has limited capacity in dealing with high temperatures and water deficits, which can also increase susceptibility to plant pathogens and low-quality kernel production (Grant & Shackel, 1998; Lampinen *et al.*, 2005; Rosati *et al.*, 2006). Wild germplasm collections can serve as a valuable resource to increase genetic variability to improve tolerance to abiotic and biotic stressors and crop productivity. The diverse *J. regia* collection at the USDA-ARS National Clonal Germplasm Repository (NCGR) located in Winters, CA, USA holds such potential. However, to date this collection has not been exploited to identify genotypes with increased abiotic stress tolerance and physiological traits related to enhanced yield.

70   Photosynthesis is a key determinant of crop productivity and positively related to biomass

71   accumulation and yield production (Fischer *et al.*, 1998; Kruger & Volin, 2006; Long *et al.* 2006;

72   Simkin *et al.* 2019; Faralli & Lawson, 2020). Photosynthetic CO_2 response curves (A_n-C_i) (net

73   assimilation, A_n versus CO_2 inside the leaf, C_i) can be used to assess the biochemical and diffusive

74   limitations that determine photosynthetic rates (Sharkey 2016; Long & Bernacchi, 2003). The

75   biochemical limitations are determined from the maximum carboxylation rate of RUBISCO

76   (V_{cmax}), the maximum rate of electron transport (J_{max}), and the maximum rate of triose phosphate

77   use (TPU), all derived from A_n-C_i curves. When combined with chlorophyll fluorescence

78   measurements, A_n-C_i curves can also provide information on diffusive limitations associated with

79   mesophyll conductance (g_m; Harley *et al.,* 1992), which is a measure of the ease with which CO_2

80   diffuses from the substomatal cavity to the site of carboxylation inside chloroplasts. Recently,

81   these biochemical characteristics have been used to evaluate germplasm in crop breeding programs

82   (De Souza & Long, 2018; De Souza *et al.*, 2020).

83   Diffusive limitations can also be used to improve photosynthesis, and are strongly linked

84   to g_m and leaf structure (Tosens *et al.*, 2012; Tomás *et al.*, 2013). g_m involves a complex pathway

85   and a series of resistances in both the gas and liquid phases (Flexas *et al.,* 2008; Tosens & Laanisto,

86   2018), and is impacted by various leaf structural traits including intercellular airspace volume (i.e.

87   porosity), mesophyll surface area exposed to the intercellular airspace (SA_{mes}/V_{mes}), mesophyll cell

88   diameter and density, and cell wall thickness (Flexas *et al.,* 2008; Flexas *et al.,* 2012; Théroux-

89   Rancourt & Gilbert, 2017; Evans 2020). Leaf structure of some species exhibits plasticity in

90   response to the growth environment (Salk 2012), resulting in functional variation, which can help

91   optimize resource use (Wright *et al.*, 2014; Muir *et al.*, 2017). Any inherent variation in leaf

92   structural and physiological traits, as a function of the habitat environment, may play an important

93   role in regulating photosynthetic capacity in *Juglans regia* accessions. We also recently found that

94   two *Juglans* spp. exhibit changes in mesophyll structure under dehydration associated with

95   changes in cell volume, orientation and arrangement that increases porosity (Momayyezi *et al.*

96   under review). Desiccation influences CO_2 diffusion and water relations as mesophyll cell turgor

97   changes (Scoffoni *et al.,* 2014; Buckley *et al.,* 2015). How genotypic diversity in mesophyll cell

98   packing and distribution across *J. regia* accessions may link with photosynthetic performance and

99   susceptibility to drought is yet to be investigated. X-ray microcomputed tomography (microCT)

100   provides an in-depth assessment of leaf mesophyll traits (i.e., porosity and tortuosity) and cells

101   orientation and geometry (Earles *et al.,* 2018; Earles *et al.,* 2019; Lundgren & Fleming, 2020;

102   Théroux-Rancourt *et al.,* 2020).

103   In this study, we combined gas exchange physiological analysis with microCT imaging of

104   leaves to explore: 1) the photosynthetic capacity of numerous *J. regia* wild accessions originating

105   from habitats with varied climatic conditions; 2) links between leaf structural diversity and

106   physiological features that enhance photosynthetic capacity; and 3) whether genotypic differences

107   hold up under water stress conditions. Based on our previous observations for two *Juglans* species

108   (Momayyezi *et al.* in review), we hypothesize that greater A_n will be associated with thicker leaves

109   and higher mesophyll porosity and gas phase diffusion (g_{IAS}) (Tomás *et al.*, 2013; Han *et al.*, 2018).

110   We also expect accessions originating from lower latitudes, characterized by warmer and wetter

111   habitats, would exhibit higher inherent A_n concurrent with higher intercellular airspace and

112   conductance as temperature and precipitation are known to strongly influence functional diversity

113   of photosynthesis across species (Ordonez & Svenning, 2017; Harrison *et al.*, 2020).

114

115   **Materials and Methods**

116   Stems were collected from 11 genetically unique *J. regia* accessions (Figs. 1A, 1B) at the

117   USDA-ARS-NCGR in Wolfskill Experimental Orchard, Winters, California USA to use as scion,

118   and were grafted by Sierra Gold Nursery onto a commonly used commercial rootstock, RX1 (*J.*

119   *microcarpa* × *J. regia*). We used a common rootstock to eliminate any own-root effects and to

120   simulate conditions for a commercial walnut orchard setting, where rootstocks are commonly used.

121   The grafted saplings were repotted and transferred to the Armstrong lathe house facility at the

122   University of California, Davis in June 2019, and kept under natural light and temperature.

123   Measurements were initiated on non-stressed plants in August 2019 under well-watered

124   conditions for all accessions. The measurements on the same plants were repeated under

125   dehydrated condition through a gradual dry down procedure using the methods as described by

126   Knipfer *et al.* (2020). Briefly, water lost from pots via transpiration and soil evaporation were

127   quantified during the experiment by weighing pots to calculate the required amount of water

128   needed per pot under each treatment, daily. After completion of measurements in non-stressed

129   conditions, water application was reduced to 75% of full-irrigation during the first week and then

130   to 50% of full-irrigation in the second week of drying. This watering regime was then maintained

131   for the dehydration treatment until completion of the experiment. Plants were maintained under

132   ambient natural light with a ~15-hour photoperiod during the experiment, maximum temperature

133   of 35°C during day and minimum of 15°C during night, in 2.65-L pots containing a 40% pine bark,

134   40% sphagnum peat moss and 20% vermiculite. The two irrigation treatments were maintained for

135   approximately two weeks prior to the measurements.

136

137   *Photosynthetic Measurements*

138   Net assimilation rate (A_n), stomatal conductance (g_s) and the intercellular airspace CO_2

139   concentration (C_i) were measured on the 4th or 5th leaflet of the most recent fully expanded leaf

140   using a LI-COR 6800 system fitted with 6800-01A fluorometer. All measurements were done

141   under PPFD = 1500 (10% blue vs. 90% red) ($\mu mol\ m^{-2}\ s^{-1}$), chamber temperature at 25°C, ambient

142   chamber CO_2 concentration (C_a) at 400 ($\mu mol\ mol^{-1}$), flow rate at 500 ($\mu mol\ air\ s^{-1}$), and vapor

143   pressure deficit between 1.5-2.0 kPa. All leaflets were dark adapted for 20 minutes prior to all

144   other measurements to obtain the maximum quantum yield of photosystem II. The quantum yield

145   of photosystem II (Φ_{PSII}) under actinic light was obtained by application of saturating multiphase

146   flashes (>8000 $\mu mol\ m^{-2}\ s^{-1}$) as per Genty *et al.* (1989).

147

148   *Calculation of g_m by Chlorophyll Fluorescence and of CO_2 Concentration in the Chloroplast (C_c)*

149   The "constant J method" was used to estimate g_m based on calculation of electron transport

150   rate (J_{flu}) from measurements of chlorophyll fluorescence (Bongi & Loreto, 1989; Harley *et al.*,

151   1992):

152    $$J_{flu} = \Phi_{PSII} \times PPFD \times \alpha \times \beta \qquad (1)$$

153   where β (= 0.5 for C_3 plants) is the fraction of absorbed quanta reaching photosystem II (Bernacchi

154   *et al.*, 2002). The leaf absorbance, α, was measured to be 85.3% based on the average value ($\pm$ 0.2

155   standard error) in all individuals using an ASD Fieldspec spectroradiometer (ViewSpec Pro, ASD

156   Inc. Boulder, CO, USA). g_m was given by (Harley *et al.*, 1992):

157    $$g_m = A_n / \left[C_i - \left(\frac{\Gamma^* \left(J_{flu} + 8(A_n + R_d) \right)}{J_{flu} - 4(A_n + R_d)} \right) \right] \qquad (2)$$

158   where R_d is the non-photorespiratory respiration rate in the light, and Γ^* is the chloroplast CO_2

159   photocompensation point. Γ^* was assumed to equal the intercellular CO_2 photocompensation point

160   (C_i^*) per Gilbert *et al.* (2012). R_d (0.73 ± 0.08 µmol m^{-2} s^{-1}) and C_i^* (38.18 ± 0.47 µmol mol^{-1})

161   were estimated using the Laisk method (Laisk, 1977 in Gilbert *et al.,* 2012) as the point of

162   intersection of the linear portion of averaged four sets of A_n-C_i curves obtained at three irradiances

163   (100, 200 and 500 µmol m^{-2} s^{-1}) and 13 CO_2 concentrations (35, 40, 50, 60, 70, 80, 90, 100, 110,

164   120, 140, 160, and 180 µmol mol^{-1}). Having obtained g_m by the chlorophyll fluorescence method,

165   the CO_2 concentration in the chloroplast (C_c) was estimated according to Harley *et al.,* (1992):

166
$$C_c = C_i - \frac{A_n}{g_m} \tag{3}$$

167   *A_n-C_i Curves*

168   To better understand photosynthetic responses, we constructed CO_2 response (A_n-C_i)

169   curves for each accession at 1500 µmol m^{-2} s^{-1} PPFD under the following sample CO_2

170   concentration: 400, 50, 80, 100, 150, 200, 400, 600, 800, 1000, 1200, 1500 ppm under well-

171   watered and dehydrated conditions. g_m obtained from the chlorophyll fluorescence method was

172   verified against g_m estimated using A_n-C_i method (Supporting Information, Fig. S2).

173

174   *Leaflet Water Potentials*

175   Leaflet water potential ($\Psi_{leaflet}$) was measured using a pressure chamber (PMS Instrument

176   Company, Model 1505D) immediately after gas exchange measurements between 10 AM to 12

177   PM (Williams & Araujo, 2002). The two leaflets opposite the one used for gas exchange

178   measurements were used to measure water potentials. The first leaflet was cut at petiolule base

179   and bagged for 10 mins to allow equilibration within the leaflet. Then, using a razor blade ~1 cm

180   of leaflet lamina was cut from either side of the middle vein to fit the short petiolule inside the

181   pressure chamber gasket. Chamber pressure was increased slowly until the balancing pressure was

182   reached. The second leaflet was covered in a dark bag for 20 mins prior to removal to obtain the

183   water potential of the rachis for the remainder of the leaf.

184

185   *X-ray Micro Computed Tomography Imaging*

186   Leaves from each accession and treatment were scanned using X-ray micro-computed

187   tomography (microCT) at beamline 8.3.2 at the Advanced Light Source (ALS) in Lawrence

188   Berkeley National Laboratory (LBNL), Berkeley, CA USA. The same leaflet samples used for gas

189   exchange were collected from the plants, bagged and placed in a cooler at room temperature an

190   hour prior to scanning in ALS. Leaves from the well-watered conditions were collected and

191   scanned in September 2019. After the plants went through the dehydration process, leaves were

192   similarly collected and scanned at ALS in October 2019. A single piece of 3 mm-wide and 7 mm-

193   long was taken from middle of the leaflet lamina from each plant and enclosed between two pieces

194   of Kapton tape to prevent desiccation of the tissue and sample movement during the scanning.

195   Samples were placed inside the end of a pipette tip and scanned under a continuous tomography

196   mode at 23 keV using 10× objective lens with a pixel resolution of 0.65 μm. Raw tomographic

197   data were reconstructed using TomoPy (Gürsoy *et al.,* 2014) through both gridrec and phase

198   retrieval reconstruction (Davis *et al.,* 1995; Dowd *et al.,* 1999).

199

200   *Mesophyll Surface Area, Porosity, Tortuosity and Lateral Path Lengthening*

201   Mesophyll porosity, θ_{IAS} (m^3 m^{-3}) was calculated as the intercellular airspace (IAS) volume

202   as a fraction of the total mesophyll volume as described by Théroux-Rancourt *et al.* (2017). The

203   IAS volume (V_{IAS}) to mesophyll cell volume ($V_{mes\text{-}cell}$) ratio and the mesophyll surface area

204   exposed to the IAS (SA_{mes}) per mesophyll volume (V_{mes}) were calculated as $V_{IAS}/ V_{mes\text{-}cell}$ (m^3 m^{-3})

205   and SA_{mes}/V_{mes} (μm^2 μm^{-3}), respectively.

206   The tortuosity factor, τ (m^2 m^{-2}), was the diffusive path length within the IAS (i.e. the

207   actual path from the stomate to a cell surface; geodesic distance [L_{geo}]) to the straight path length

208   without any physical obstacles to diffusion between the stomate and the cell surface (Euclidean

209   distance, L_{Euc}):

$$\tau = (\frac{L_{geo}}{L_{Euc}})^2 \tag{4}$$

211   as described in Earles *et al.,* (2018). The L_{geo} and L_{Euc} were mapped and quantified for all voxels

212   along the mesophyll surface and τ was calculated for the whole 3D image array as in Earles *et al.*

213   (2018). Then, leaf-level tortuosity (τ_{leaf}) was calculated as the mean of τ values at the edge of

214   mesophyll cells. The lateral path lengthening, λ (m m^{-1}) was calculated using L_{Euc}, and a second

215   distance map as described by Earles *et al.* (2018) to measure the shortest unobstructed distance in

216   a straight line between the abaxial epidermis and all points along the mesophyll surface, L_{epi}

217   (Legland *et al.,* 2016):

$$\lambda = \frac{L_{Euc}}{L_{epi}} \tag{5}$$

219   Similarly, leaf-level lateral path lengthening (λ_{leaf}) was then calculated as the mean of λ values at

220   the edge of mesophyll cells.

221

IAS Conductance and Stomatal Density

The τ_{leaf}, λ_{leaf}, and θ_{IAS} were used to calculate leaf-level IAS conductance (g_{IAS}), where D_m is the diffusivity of CO_2 in air (m^2 s^{-1}). Diffusion path length in gas phase was equal to half of the mesophyll thickness (L_{mes}) for hypostomatous leaves (Niinemets & Reichstein, 2003; Tomás *et al.*, 2013; Earles *et al.*, 2018):

$$g_{IAS} = \frac{\theta_{IAS}\, D_m}{0.5 L_{mes} \tau_{leaf} \lambda_{leaf}} \tag{6}$$

As a parallel method was used to verify auto-segmentation and IAS trait estimation by random forest model. A PyTorch implementation of a fully convolutional network model with a ResNet-101 backbone was used for the semantic segmentation of the leaf image data with cloud-based resources in Google Colab. For training, we used a binary cross-entropy loss function, an Adam optimizer for stochastic optimization with a learning rate of 0.001, a scaling factor of 1 to avoid small feature loss in the training images, and a batch size of 1 to accommodate the GPU limitations in Google Colab. Output results were comparable to those generated on the same image sets with a workflow developed by Théroux-Rancourt *et al.* (2020) using a random forest model for semantic segmentation of leaf tissues. The output was used to validate tissue surface area and volume determination and 3-D leaf projection (Supporting Information, Fig. S3).

To quantify the stomatal density, the grid reconstructions were used at the paradermal direction. The stomata density and size were measured in 0.04 mm^2 for all the leaves.

Climatic Data for Accessions' Native Habitats

Coordinates for each accession's native habitats were extracted from the USDA-ARS GRIN (Germplasm Resources Information Network) database (https://npgsweb.ars-

244   grin.gov/gringlobal/search). Temperature and precipitation data were obtained from FAO climate

245   information tools (https://aquastat.fao.org/climate-information-tool/) for each of these native

246   habitat locations (Supporting Information, Fig. S1).

247

248   *Statistics*

249   Linear regression and Pearson correlation coefficients were used to examine relationships

250   between latitude, temperature and precipitation seasonality, frost-free days, and A_n, A_{max} g_s, g_m,

251   g_{IAS}, L_{leaf}, θ_{IAS}, λ_{leaf}, τ, Leaf N, LMA, J_{max}, V_{cmax}, $\Psi_{leaflet}$ using GraphPad prism 9 software

252   (GraphPad Software, Inc. CA, USA). Paired *t*-test was used to check for systematic differences

253   between the chlorophyll fluorescence and A_n-C_i curve methods for estimating g_m and C_c. Mixed

254   linear models were used to compare relative changes in percent for A_n, g_m, g_s, L_{leaf}, g_{IAS}, θ_{IAS}, $\Psi_{leaflet}$

255   under dehydration for all accessions using SAS 9.4 (SAS Institute Inc. NC, USA 2013). The *P*

256   value required for significance (0.002) was adjusted by dividing α (0.05) by the number of

257   comparisons per test (twenty-five, here). Logarithm or squared transformations were performed to

258   meet normality and equal variance assumptions where needed.

259

260   **Results**

261   Inherent differences in photosynthetic capacity were found among the accessions; *J. regia*

262   accessions 3, 5 and 9 showed the highest photosynthetic capacity, as measured by A_{max} (26.3, 25.6,

263   27.5 μmol CO_2 m^{-2} s^{-1}, respectively). Higher A_{max} in these accessions was linked to greater

264   maximum carboxylation rate (V_{cmax}, $R^2 = 0.81$, $P <0.001$) and maximum electron transport rate

265   (J_{max}, $R^2 = 0.67$, $P =0.002$) (Fig. 3, Supporting Information, Fig. S5). Leaves with higher A_{max} had

266 thicker leaves (L_{leaf}, $P = 0.013$) with greater mesophyll porosity (θ_{IAS}, $P = 0.049$) and leaf nitrogen

267 (Leaf N, $P = 0.044$) (Supporting Information, Fig. S5).

268   Similarly, A_n was positively correlated with g_s ($P = 0.034$) (Fig. 4) across the accessions.

269 Similar to A_{max}, leaves with greater A_n were thicker (L_{leaf}, $P = 0.037$) with more mesophyll (L_{mes},

270 $P = 0.05$) and higher mesophyll porosity (θ_{IAS}, $P = 0.041$) and nitrogen content per unit area (leaf

271 N, $P = 0.012$) but less leaf mass per unit area (LMA, $P = 0.007$) (Fig. 4). Increased A_n was not

272 significantly related with lateral path lengthening (λ_{leaf}, $P = 0.091$) nor tortuosity (τ_{leaf}, $P > 0.1$)

273 (data not presented). Leaves with greater θ_{IAS} exhibited higher thickness ($R^2 = 0.36$; $P = 0.048$),

274 and had greater g_m ($P = 0.03$) and lower λ_{leaf} ($P = 0.03$) (Supporting Information, Fig. S6), and g_s

275 ($P = 0.0003$), concurrent with lower stomatal density ($R^2 = 0.38$; $P = 0.042$). Across accessions,

276 leaflet water potential ($\Psi_{leaflet}$) was positively related to both θ_{IAS} ($P = 0.024$) and g_s ($P = 0.028$).

277

278 *Climate-Driven Photosynthetic Capacity*

279   Photosynthetic capacity and associated leaf physiological and anatomical characteristics

280 for the accessions were partially driven by climatic conditions in association with native habitats.

281 Accessions from habitats with lower temperature seasonality in lower latitudes had higher g_{ias} and

282 leaf N ($P \leq 0.05$), which may support higher their A_n through greater g_m and θ_{IAS} (Fig. 5; $P = 0.05$,

283 Supporting Information, Fig. S4). Despite non-significant relationships, parallel decreases in g_m,

284 g_{IAS}, leaf N, and θ_{IAS} ($P > 0.05$) (Supporting Information, Fig. S4) may suggest a pattern for decline

285 in mesophyll CO_2 diffusion with latitude, while they accumulate more LMA ($P = 0.015$) (Fig. 5).

286 Higher variability in precipitation seasonality and more frost-free days were significantly related

287   to increased g_{IAS} concurrent with lower stomatal density (Fig. 5). Decreases in LMA and frost-free

288   days were associated with increases in leaf N (Fig. 5).

289

290   *Responses under Dehydration*

291   As expected, dehydration impaired photosynthesis and altered leaf structure with reduced

292   g_s, g_m, and L_{leaf} and increased θ_{IAS} and g_{IAS} in all accessions. The percent reduction in A_n was

293   significantly correlated with percent reductions in g_s ($P = 0.007$), g_m ($P = 0.002$), and $\Psi_{leaflet}$ ($P =$

294   0.002) under dehydration (Table 1). Accessions A3, A5, and A9, which had the highest A_n and

295   A_{max} under well-watered conditions, exhibited the greatest percent reductions amongst accessions

296   in these parameters under drought stress (i.e. >50% reduction for all three; Table 1). However, the

297   absolute values of A_n for accessions A3 and A5 were not significantly lower than other accessions

298   under dehydration, while they were amongst the lowest for A9 under dehydration (Table S2). The

299   reduction in L_{leaf} was linked with decreases in g_{ias} ($P = 0.02$) and g_m ($P = 0.08$). The concurrent

300   reduction in $\Psi_{leaflet}$ was significantly correlated with percent decline in g_s ($P = 0.004$) (Table 1).

301   Under dehydration, absolute A_n, g_m, θ_{IAS}, g_{IAS}, and leaf N remained negatively correlated with

302   latitude ($P < 0.05$, Table 2).

303

304   **Discussion**

305   *Photosynthetic Capacity, Mesophyll Anatomy, and CO$_2$ Diffusion*

306   Diverse accessions of *J. regia*, native to various habitats with different temperature and

307   precipitation patterns, exhibited variable photosynthetic capacity. Three accessions (A3, A5, and

308   A9) exhibited significantly higher A_n, A_{max} and CO_2 diffusion capacity under the well-watered

309   condition associated with the highest combined values of V_{cmax} and J_{max}. Greater photosynthetic

310   capacity is typically linked to carboxylation capacity via increased Rubisco protein abundance and

311   activity (von Caemmerer & Farquhar, 1981; Hikosaka & Shigeno, 2009; Díaz *et al.*, 2011). All

312   accessions exhibited significant reductions in photosynthesis under dehydration, A3 and A5 still

313   exhibited similar absolute values under stress.

314   Higher photosynthetic capacity was strongly linked to leaf thickness and mesophyll

315   structure and supported by higher leaf N. As expected, *J. regia* accessions with thicker leaves

316   exhibited greater θ_{IAS}, g_{IAS}, g_m and A_n (Fig. 4). This agrees with previous findings for *J. regia* cv.

317   Chandler (Momayyezi *et al.*, *in review*). *J. regia* accessions with higher A_n had greater A_{max}, V_{cmax}

318   and leaf N suggesting higher carboxylation capacity and performance (Fig. 3, Supporting

319   Information, Fig. S5). While previous work reported a positive relationship between A_n with LMA

320   (i.e. across *Quercus ilex* provenances; Peguero-Pina *et al.*, 2017), we found *J. regia* accessions

321   exhibited greater A_n with lower LMA. Increasing cell density would reduce mesophyll surface

322   area exposed to IAS as a result of high cell packing and could also be impacted by cell wall

323   thickness (Niinemets *et al.*, 2009; Tosens *et al.*, 2012; Tomás *et al.*, 2013). A more porous

324   mesophyll and thicker leaves with shorter λ_{leaf} (Supporting Information, Fig. S6), resulted in higher

325   A_{max} across *J. regia* accessions (Supporting Information, Fig. S5), highlighting the fact that

326   thickness and cell density may not change in the same direction (Syversten *et al.*, 1995; Niinemets

327   *et al.*, 1999). Increases in leaf porosity are known to reduce diffusive resistance and lateral path

328   lengthening in other species (Earles *et al.*, 2018). Additionally, leaf mesophyll geometry and IAS

329   are known to impact stomatal patterning, photosynthetic capacity, and conductances (Baillie &

330 Fleming 2017; Graham *et al.*, 2017; Lundgren *et al.*, 2019); *J. regia* accessions with greater

331 porosity had fewer but larger stomata with significantly greater g_s.

332   Leaf anatomy also plays an important role in biophysical coordination between CO_2

333 diffusion and leaf hydraulics (Boyce *et al.*, 2009; Graham *et al.*, 2017; Rockwell & Holbrook,

334 2017). Similar to findings from Trueba *et al.* (2021), *J. regia* accessions with greater porosity had

335 fewer veins per leaf volume ($P = 0.049$) and lower WUE_i ($P = 0.047$) associated with higher g_s.

336 More extensive vasculature, including greater bundle sheath extensions, may improve WUE_i by

337 improving connections between the vascular tissue and epidermis for stomatal regulation and

338 water supply to replace losses due to transpiration (Brodribb *et al.*, 2007; Zwieniecki *et al.*, 2007).

339

340 *Climatic Variables and Inherent Functional Diversity*

341   We found inherent differences in the photosynthetic activity of *J. regia* accessions is

342 associated with climatic conditions in their native habitat (Fig. 5, Supporting Information, Fig. S4).

343 Other studies have shown that leaf structure and function are strongly related to the environment

344 of a species' native habitat (Reich 2014; Li *et al.*, 2018). Higher precipitation seasonality,

345 concurrent with more frost-free days in lower latitudes, resulted in higher A_n through increased g_m

346 and g_{IAS}. This can be due to increased allocation of leaf N toward the dynamic biochemical activity

347 rather than more static aspects of the mesophyll (e.g., wall thickness and mesophyll surface area)

348 (Terashima *et al.*, 2006; Tosens *et al.*, 2012; Evans 2020). As discussed by He *et al.* (2016),

349 changes in leaf anatomy (i.e. leaf and epidermis thickness and the ratio of spongy to palisade

350 mesophyll) as a function of latitude are mainly driven by variability in precipitation and

351 temperature. *J. regia* accessions from habitats from lower latitudes with lower temperature

352 seasonality had leaves with greater g_{IAS} and tortuosity. Greater precipitation during the warmest

353 annual quarter (between June-August), when *J. regia* has the highest water demand for growth and

354 fruit development, was associated with increased g_{IAS} ($P = 0.02$) and reduced SD ($P < 0.001$)

355 suggesting a potential positive impact of irrigation on leaf performance by improving CO_2

356 diffusion.

357 On the other hand, the photosynthetic performance seems to be unrelated to the

358 phylogenetic history. Accessions with greater A_n and A_{max}, like A3 and A9, share a close

359 evolutionary background with low-performance accessions, like A4 and A11, but not with each

360 other (Fig. 1B). Therefore, unlike studies that reported strong phylogenetic support for water stress

361 resistant traits like xylem cavitation vulnerability in stem and root (Wilson *et al.*, 2008), vein

362 development, patterning and hydraulic conductance (Brodribb *et al.*, 2007), our results suggest

363 that geographical variability is more strongly linked with differences in photosynthetic rate in

364 *Juglans* accessions.

365 Leaf nitrogen content per unit area (leaf N) was negatively related to latitude and supported

366 higher A_n with greater biochemical activity. Increases in A_n related to changes in leaf N and

367 chlorophyll content have been reported for *Populus balsamifera* and *P. angustifolia* populations

368 as an adaptive response to growing season length (Soolanayakanahlly *et al.*, 2009; Kaluthota *et*

369 *al.*, 2017). Latitudinal variation in photosynthetic variables have been reported more broadly

370 across various species, however, the patterns were opposite in *Populus* spp. For example,

371 latitudinal increases in A_n and for *P. trichocarpa* genotypes was accompanied by greater g_m

372 through higher CA activity and aquaporins functioning that were attributed to growth under shorter

373 growing season in northern habitats (Gornall & Guy, 2007; McKown *et al.*, 2014; Momayyezi &

374 Guy, 2017; Momayyezi & Guy, 2018).

375

Dehydration Induced Responses

377   As expected, dehydration negatively impacted photosynthesis in all accessions, but some

378 exhibited greater reductions in A_n with decreases in g_m, g_s, and $\Psi_{leaflet}$ ($P = 0.007$). Accessions A3,

379 A5 and A9 exhibited the highest photosynthetic capacity, but also had the highest % reductions

380 due to drought. A reduction in photosynthesis under dehydration was associated with decreases in

381 PSII efficiency, which could be due to increases in photorespiration associated with increased

382 resistance to CO_2 diffusion through stomata and mesophyll (Sharkey 1988; Lima Neto *et al.*, 2017;

383 Busch 2020). Even under dehydration, accessions A3 and A5 from lower latitudes maintained

384 higher A_n, g_m, θ_{IAS}, g_{IAS}, and leaf N (Table 2), suggesting that these accessions hold potential for

385 commercial production without increasing susceptibility to stress in absolute terms.

386   Dehydration reduced leaf thickness and increased θ_{IAS} and g_{IAS} by shrinking mesophyll cell

387 size more than IAS (Tables 1 and S2); this is consistent with our earlier observations for *J. regia*

388 cv. Chandler and *J. microcarpa* (Momayyezi *et al.*, under review). In the current study, g_{IAS}

389 increased by 13-35% in different *J. regia* accessions under dehydration. However, its contribution

390 to g_m was 7-23% under well-watered but decreased to 3-8% under drought across accessions,

391 which is within the expected limiting range (3-37%) for woody perennial species with

392 hypostomatous leaves (Parkhurst & Mott, 1990; Niinemets & Reichstein, 2003; Tosens *et al.*,

393 2012; Tomás *et al.*, 2013; Harwood *et al.*, 2021). Additionally, reductions in the g_{IAS} contribution

394 to g_m was closely and positively related to A_n ($R^2 = 0.63$; $P = 0.003$) and A_{max} ($R^2 = 0.37$; $P = 0.044$),

395 suggesting reduced gas phase diffusion under stress may decrease photosynthesis further by

396 limiting CO_2 diffusion in liquid phase through chloroplast re-positioning and activity of carbonic

397 anhydrases and aquaporins (Tholen *et al.*, 2008; Miyazawa *et al.*, 2008; Evans *et al.,* 2009; Tomás

398 *et al.*, 2013; Momayyezi *et al.*, 2020).

399

Conclusions

401   We found that photosynthetic capacity in *J. regia* accessions was associated with leaf

402 anatomical and biochemical components that impact CO_2 diffusion. Leaves with greater porosity

403 and g_{IAS} contribution to g_m exhibited the highest photosynthetic capacity at ambient and saturating

404 CO_2. Improved photosynthesis was supported by increased carboxylation capacity and leaf

405 nitrogen accumulation. Higher photosynthesis across accessions was associated with frost-free

406 days and precipitation and temperature seasonality patterns in low-latitude native habitats.

407 Although *J. regia* has a limited resilience under dehydration, two of the low-latitude accessions

408 (e.g. A3 and A5) with the highest inherent photosynthetic capacity, sustained performance under

409 stress. These accessions hold promise for high productivity and use in breeding programs for

410 commercial walnut production.

411

420

421   **Conflict of Interest**

422   None to report.

423

424

425

426

Literature Cited

Baillie AL, Fleming AJ. 2020. The developmental relationship between stomata and mesophyll airspace. *New Phytologist* **225:** 1120-1126.

Bernacchi CJ, Portis AR, Nakano H, von Caemmerer S, Long SP. 2002. Temperature response of mesophyll conductance; implications for the determination of rubisco enzyme kinetics and for limitations to photosynthesis *in vivo*. *Plant Physiology* **130:** 1992-1998.

Bongi G, Loreto F. 1989. Gas-exchange properties of salt-stressed olive (*Olea europea* L.) leaves, *Plant Physiology* **90:** 1408-1416.

Boyce CK, Brodribb TJ, Feild TS. Zwieniecki MA. 2009. Angiosperm leaf vein evolution was physiologically and environmentally transformative. *Proceedings of the Royal Society B.* **276:** 1771-1776.

Brodribb TJ, Field TS, Jordan GJ. 2007. Leaf maximum photosynthetic rate and venation are linked by hydraulics. *Plant Physiology* **144:** 1890-1898.

Busch FA. 2020. Photorespiration in the context of Rubisco biochemistry, CO_2 diffusion and metabolism. *Plant Journal* **101:** 919-939.

Buckley TN, John GP, Scoffoni C, Sack L. 2017. The sites of evaporation within leaves. *Plant Physiology* **173:** 1763-1782.

von Caemmerer S, Farquhar GD. 1981. Some relationships between the biochemistry of photosynthesis and the gas exchange of leaves. *Planta* **153:** 376-387.

Carnis Murphy MR, Jordan GJ, Brodribb T. 2014. Acclimation to humidity modifies the link between leaf size and the density of veins and stomata. *Plant, Cell and Environment* **37:** 124-131.

Clay K, Quinn JA. 1978. Density of Stomata and Their Responses to a Moisture Gradient in Danthonia sericea Populations from Dry and Wet Habitats. *Bulletin of the Torrey Botanical Club.* **105:** 45-49.

Davis TJ, Gao D, Gureyev TE, Stevenson AW, Wilkins SW. 1995. Phase contrast imaging of weakly absorbing materials using hard X-rays. *Nature* **373**: 595-598.

De Souza AP, Long SP. 2018. Toward improving photosynthesis in cassava: characterizing photosynthetic limitations in four current African cultivars. Food Energy Security 7: e00130.

De Souza AP, Wang Y, Orr DJ, Carmo-Silva E, Long SP. 2020. Photosynthesis across African cassava germplasm is limited by Rubisco and mesophyll conductance at steady state, but by stomatal conductance in fluctuating light. New Phytol, 225: 2498-2512

Dowd BA, Campbell GH, Marr RB, Nagarkar VV, Tipnis SV, Axe L, Siddons DP. 1999. Developments in synchrotron x-ray computed microtomography at the National Synchrotron Light Source. In: U Bonse, ed, SPIE's International Symposium on Optical Science, Engineering, and Instrumentation. SPIE, pp 224-236 10.1117/12.363725.

Duke JA. 1978. The Quest for Tolerant Germplasm. *In* Crop Tolerance to Suboptimal Land Conditions, GA. Jung (Ed.). https://doi.org/10.2134/asaspecpub32.c1

Earles JM, Théroux-Rancourt G, Roddy AB, Gilbert ME, McElrone AJ, Brodersen CR. 2018. Beyond porosity: 3D leaf intercellular airspace traits that impact mesophyll conductance. *Plant Physiology* **178:** 148-162.

Earles, J M, Buckley TN, Brodersen CR, Busch FA, Cano FJ, Choat B, Evans JR, et al. 2019. Embracing 3D complexity in leaf carbon–water exchange. *Trends in Plant Science* **24:** 15-24.

Evans J.R., Kaldenhoff R., Genty B. & Terashima I. 2009. Resistances along the CO_2 diffusion pathway inside leaves. *Journal of Experimental Botany* **60:** 2235-2248.

Evans JR. 2021. Mesophyll conductance: walls, membranes and spatial complexity. *New Phytologist* doi: org/10.1111/nph.16968.

Faralli, M. Lawson, T. 2020. Natural genetic variation in photosynthesis: an untapped resource to increase crop yield potential? *The Plant Journal* **101:** 518-528.

Fischer, RA, Rees D, Sayre KD, Lu ZM, Condon AG, Saavedra AL. 1998. Wheat yield progress associated with higher stomatal conductance and photosynthetic rate, and cooler canopies. *Crop Science* **38:** 1467-1475.

481   **Flexas J, Ribas-Carbó M, Diaz-Espejo A, Galmés J, Medrano H. 2008.** Mesophyll
482   conductance to CO_2: current knowledge and future prospects. *Plant, Cell and Environment*
483   **31:** 602-621.

484   **Flexas J, Barbour MM, Brendel O, Cabrera HM, Carriquí M, Díaz-Espejo A, Douthe C,**
485   **Dreyer E, Ferrio JP, Gago J, Gallé A, Galmés J, Kodama N, Medrano H, Niinemets**
486   **Ü, Peguero-Pina JJ, Pou A, Ribas-Carbó M, Tomás M, Tosens T, Warren CR. 2012.**
487   Mesophyll diffusion conductance to CO_2: an unappreciated central player in
488   photosynthesis. *Plant Science* **193-194:** 70-84.

489   **Genty B, Briantais JM, Baker NR. 1989.** The relationship between the quantum yield of
490   photosynthetic electron transport and quenching of chlorophyll fluorescence. *Biochimica*
491   *et Biophysica Acta* **990:** 87-92.

492   **Gilbert ME, Zwieniecki MA, Holbrook NM. 2011.** Independent variation in photosynthetic
493   capacity and stomatal conductance leads to differences in intrinsic water use efficiency in
494   11 soybean genotypes before and during mild drought. *Journal of Experimental Botany*
495   **62:** 2875-2887.

496   **Gilbert ME, Pou A, Zwieniecki MA, Holbrook NM. 2012.** On measuring the response of
497   mesophyll conductance to carbon dioxide with the variable *J* method. *Journal of*
498   *Experimental Botany* **63:** 413-425.

499   **Gornall JL, Guy RD. 2007.** Geographic variation in ecophysiological traits of black cottonwood
500   (*Populus trichocarpa*). *Canadian Journal of Botany* **85:** 1202-1213.

501   **Grant JA, Shackel K. 1998.** Influence of irrigation water deficit on stem end kernel shrivel of
502   Chandler walnuts. An annual research report submitted to the California Walnut Board.
503   https://ucanr.edu/sites/cawalnut/showyears/1998/?repository=66994&a=154103.

504   **Gürsoy D, De Carlo F, Xiao X, Jacobsen C**. **2014**. TomoPy: a framework for the analysis of
505   synchrotron tomographic data. *Journal of synchrotron radiation* **21**: 1188-1193.

506 **Han J, Lei Z, Zhang Y, Yi X, Zhang W, Zhang Y. 2019.** Drought-introduced variability of
507   mesophyll conductance in *Gossypium* and its relationship with leaf anatomy. *Physiologia*
508   *Plantarum* **166:** 873-887.

509 **Harley PC, Loreto F, Di Marco G, Sharkey TD. 1992.** Theoretical considerations when
510   estimating the mesophyll conductance to CO_2 flux by analysis of the response of
511   photosynthesis to CO_2. *Plant Physiology* **98:** 1429-1436.

512 **Harrison S, Spasojevic MJ, Li D. 2020.** Climate and plant community diversity in space and
513   time. *Proceedings of the National Academy of Sciences of the United States of America*
514   **117:** 4464-4470.

515 **Harwood R, Théroux-Rancourt G, Barbour MM. 2021.** Understanding airspace in leaves: 3D
516   anatomy and directional tortuosity. *Plant, Cell & Environment* doi:10.1111/pce.14079

517 He N**,** Liu C**,** Tian M**, Li M, Yang H, Yu G, Guo D, Smith MD, Yu Q, Hou J. 2018.** Variation
518   in leaf anatomical traits from tropical to cold-temperate forests and linkage to ecosystem
519   functions. *Functional Ecology* **32:** 10-19.

520 **Hikosaka K, Shigeno A. 2009.** The role of Rubisco and cell walls in the interspecific variation in
521   photosynthetic capacity. *Oecologia* **160:** 443-451.

522 **Kaluthota S, Pearce DW, Evans LM, Letts MG, Whitham TG, Rood SB. 2015.** Higher
523   photosynthetic capacity from higher latitude: foliar characteristics and gas exchange of
524   southern, central and northern populations of *Populus angustifolia*. *Tree Physiology* **35:**
525   936-948.

526 **Kattge J, Díaz S, Lavorel S, et al. 2011.** TRY-a global database of plant traits. *Global Change*
527   *Biology* **17:** 2905-2935.

528 **Kluepfel D, Leslie C, Aradhya M, Browne G, et al. 2015.** Development of disease-resistant
529   walnut root stocks: Integration of conventional and genomic approaches. Walnut Research
530   Reports pg 87- 91. http://ucanr.edu/repositoryfiles/2015-087-160265.pdf.

531 **Knipfer T, Reyes C, Momayyezi M, Brown PJ, Kluepfel D, McElrone AJ. 2020.** A
532   comparative study on physiological responses to drought in walnut genotypes (RX1,
533   Vlach, VX211) commercially available as rootstocks. *Trees* **34:** 665-678.

534 **Kruger EL, Volin JC. 2006.** Reexamining the empirical relation between plant growth and leaf
535   photosynthesis. *Functional Plant Biology* **33:** 421-429.

536 **Lampinen B, Hasey J, Metcalf S, Negrón C. 2005.** Irrigation management as a tool to stabilize
537   and revitalize a declining 'chandler' orchard. An annual research report submitted to the
538   California Walnut Board for 2005.
539   https://ucanr.edu/sites/cawalnut/AuthorsMR/MetcalfS/?repository=70834&a=154390.

540 **Legland D, Arganda-Carreras I, Andrey P. 2016.** MorphoLibJ: integrated library and plugins
541   for mathematical morphology with ImageJ. *Bioinformatics* **32**: 3532-3534.

542 **Leslie CA, and McGranahan, GH. 1998.** The origin of the walnut, pp. 3-7. In: Ramos, D. E.
543   (Ed.), Walnut Production Manual. University of California. Division of Agriculture and
544   Natural Resources. Publication 3373. 319 pp.

545 **Leslie C, McGranahan G, Hackett W, Martinez-Garcia PJ, Wang G, Ramasamy R, Chen**
546   **L, Walawage L, Grant J, Caprile J, Coates B, Buchner R, Hasey J, Doll D, Fichtner**
547   **E, Pope K, Dandekar A, Aradhya M, Sudarshana S, Neal D, Dvorak J. 2015.** Walnut
548   Improvement Program 2015. https://ucanr.edu/sites/cawalnut/category/genetic_breeding/

549 **Li X, Blackman CJ, Choat B, Duursma RA, Rymer PD, Medlyn BE, Tissue DT. 2018.** Tree
550   hydraulic traits are coordinated and strongly linked to climate-of-origin across a rainfall
551   gradient. *Plant, Cell and Environment* **41:** 646-660.

552 **Lima Neto MC, Cerqueira JVA, da Cunha JR, Ribeiro RV, Silveira JAG. 2017.** Cyclic
553   electron flow, NPQ and photorespiration are crucial for the establishment of young plants
554   of *Ricinus communis* and *Jatropha curcas* exposed to drought. *Plant Biology* **19:** 650-
555   659.

556 **Liu Q, Piao S, Janssens IA, Fu Y, Peng S, Lian X, Ciais P, Myneni RB, Peñuelas, Wang T.**
557   **2018.** Extension of the growing season increases vegetation exposure to frost. *Nature*
558   *Communications* **9:** 426. https://doi.org/10.1038/s41467-017-02690-y.

559 **Long SP, Zhu XG, Naidu SL, Ort DR. 2006.** Can improvement in photosynthesis increase crop
560   yields? *Plant, Cell and Environment* **29:** 315-30.

561 **Lundgren MR Mathers A, Baillie AL. Dunn J, Wilson MJ, Hunt L, Pajor R, Fradera-Soler**
562   **M, Rolfe S, Osborne CP, Sturrock CJ, Gray JE, Money SJ, Fleming AJ. 2019.**
563   Mesophyll porosity is modulated by the presence of functional stomata. *Nature*
564   *Communications* **10:** 2825. https://doi.org/10.1038/s41467-019-10826-5

565 **Marelle L, Myhre G, Hodnebrog Ø, Sillmann J, Samset BH. 2018.** The changing seasonality
566   of extreme daily precipitation. *Geophysical Research Letters* **45:** 11352-11360.

567 **McGranahan GH, Leslie CA. 2009.** Breeding walnuts (*Juglans regia*). In: Mohan Jain S,
568   Priyadarshan PM, eds. *Breeding plantation tree crops: temperate species*. New York, NY:
569   Springer, 249-273.

570 **McKown AD, Guy RD, Klápště J, Geraldes A, Friedmann M, Cronk QCB, El-Kassaby YA,**
571   **Mansfield SD, Douglas CJ. 2014a.** Geographical and environmental gradients shape
572   phenotypic trait variation and genetic structure in *Populus trichocarpa. New Phytologist*
573   *201: 1263-1276.*

574 **McKown AD, Guy RD, Quamme LA, Klápště J, La Mantia J, Constabel CP, El-Kassaby**
575   **YA, Hamelin RC, Zifkin M, Azam MS. 2014b.** Association genetics, geography and
576   ecophysiology link stomatal patterning in *Populus trichocarpa* with carbon gain and
577   disease resistance trade-offs. *Molecular Ecology* **23:** 5771-5790.

578 **Miyazawa S, Yoshimura S, Shinzaki Y, Maeshima M, Miyake C. 2008.** Deactivation of
579   aquaporins decreases internal conductance to CO_2 diffusion in tobacco leaves grown under
580   long-term drought. *Functional Plant Biology* **35:** 553-564.

581 **Momayyezi M, Guy RD. 2017.** Substantial role for carbonic anhydrase in latitudinal variation in
582   mesophyll conductance of *Populus trichocarpa* Torr. & Gray. *Plant, Cell and Environment*
583   **40:** 138-149.

584 **Momayyezi M, Guy RD. 2018.** Concomitant effects of mercuric chloride on mesophyll
585   conductance and carbonic anhydrase activity in *Populus trichocarpa* Torr. & Gray. *Trees*
586   **32:** 301-309.

587 **Momayyezi M, McKown AD, Bell SCS, Guy RD. 2020.** Emerging roles for carbonic anhydrase
588   in mesophyll conductance and photosynthesis. *The Plant Journal* **101:** 831-844.

589 **Muir CD, Conesa MÀ, Roldán EJ, Molins A, Galmés J. 2017.** Weak coordination between leaf
590   structure and function among closely related tomato species. *New Phytologist* **213:** 1642-
591   1653.

592 **Niinemets Ü. 1999.** Research review. Components of leaf dry mass per area thickness and density
593   alter leaf photosynthetic capacity in reverse directions in woody plants. *New Phytologist*
594   **144:** 35-47.

595 **Niinemets Ü, Reichstein M. 2003.** Controls on the emission of plant volatiles through stomata:
596   a sensitivity analysis. *Journal of Geophysical Research* **108**: 4211. doi:
597   10.1029/2002JD002620.

598 **Niinemets U, Wright IJ, Evans JR. 2009.** Leaf mesophyll diffusion conductance in 35
599   Australian sclerophylls covering a broad range of foliage structural and physiological
600   variation. *Journal of Experimental Botany* **60:** 2433-2449.

601 **Ordonez A, Svenning JC. 2017.** Consistent role of Quaternary climate change in shaping current
602   plant functional diversity patterns across European plant orders. *Scientific*
603   *Reports* **7,** 42988. https://doi.org/10.1038/srep42988.

604 **Parkhurst DF, Mott KA.** 1990. Intercellular diffusion limits to CO_2 uptake in leaves: studies in
605   air and helox. *Plant Physiology* **94**: 1024-1032.

606 **Pearce DW, Millard S, Bray DF, Rood SB. 2006.** Stomatal characteristics of riparian poplar
607   species in a semi-arid environment. *Tree Physiology* **26:** 211-218.

608 **Peguero-Pina JJ, Gil-Pelegrín E, Morales F. 2009.** Photosystem II efficiency of the palisade and
609   spongy mesophyll in *Quercus coccifera* using adaxial/abaxial illumination and excitation
610   light sources with wavelengths varying in penetration into the leaf tissue. *Photosynthesis*
611   *Research* **99:** 49-61.

Fulton E. Rockwell N. Holbrook M. 2017. Leaf hydraulic architecture and stomatal conductance: a functional perspective. *Plant Physiology* **174:** 1996-2007.

Reich PB. 2014. The world-wide 'fast–slow' plant economics spectrum: a traits manifesto. *Journal of Ecology* **102:** 275-301.

Rosati A, Metcalf S, Buchner R, Fulton A, Lampinen B. 2006. Tree water status and gas exchange in walnut under drought, high temperature and vapour pressure deficit. The Journal of Horticultural Science and Biotechnology, 81:3, 415-420, DOI: 10.1080/14620316.2006.11512082.

Salk C. 2012. Within-species leaf trait variation and ecological flexibility in resprouting tropical trees. *Journal of Tropical Ecology,* **28:** 527-530.

Scoffoni C, Vuong C, Diep S, Cochard H, Sack L. 2014. Leaf shrinkage with dehydration: coordination with hydraulic vulnerability and drought tolerance. *Plant Physiology* **164:** 1772-1788.

Scoffoni C, Albuquerque C, Brodersen CR, Townes SV, John GP, Bartlett MK, Buckley TN, McElrone AJ, Sack L. 2017. Outside xylem vulnerability, not xylem embolism, controls leaf hydraulic decline during dehydration. *Plant Physiology* **173:** 1197-1210.

Simkin AJ, López-Calcagno PE, Raines CA. 2019. Feeding the world: improving photosynthetic efficiency for sustainable crop production. *Journal of Experimental Botany*, **70:** 1119-1140.

Sharkey TD. 1988. Estimating the rate of photorespiration in leaves. *Physiologia Plantarum* **73:** 147-152.

Soolanayakanahally RY, Guy RD, Slim SN, Drewes EC, Schroeder WR. 2009. Enhanced assimilation rate and water use efficiency with latitude through increased photosynthetic capacity and internal conductance in balsam poplar (*Populus balsamifera* L.). *Plant, Cell and Environment* **32:** 1821-1823.

637 **Syvertsen JP, Lloyd, J, McConchie C, Kriedemann PE, and Farquhar GD. 1995.** On the

638   relationship between leaf anatomy and CO_2 diffusion through the mesophyll of

639   hypostomatous leaves. *Plant, Cell and Environment* **18:** 149-157.

640 **Terashima I, Hanba YT, Tazoe Y, Vyas P, Yano S. 2006.** Irradiance and phenotype:

641   comparative eco-development of sun and shade leaves in relation to photosynthetic

642   CO_2 diffusion. *Journal of Experimental Botany* **57:** 343-354.

643 **Tomás M, Flexas J, Copolovici L, Galmés J, Hallik L, Medrano H, Ribas-Carbó M, Tosens**

644   **T, Vislap V, Niinemets Ü. 2013.** Importance of leaf anatomy in determining mesophyll

645   diffusion conductance to CO_2 across species: quantitative limitations and scaling up by

646   models. *Journal of Experimental Botany* **64:** 2269-2281.

647 **Théroux-Rancourt G, Gilbert ME. 2017.** The light response of mesophyll conductance is

648   controlled by structure across leaf profiles. *Plant, Cell and Environment* **40:** 726-740.

649 **Théroux-Rancourt G, Earles JM, Gilbert ME, Zwieniecki MJ, Boyce CK, McElrone AJ,**

650   **Brodersen CR. 2017.** The bias of a two-dimensional view: comparing two-dimensional

651   and three-dimensional mesophyll surface area estimates using noninvasive imaging. *New*

652   *Phytologist* **215:** 1609-1622.

653 **Theroux-Rancourt G, Jenkins MR, Brodersen CR, McElrone A, Forrestel EJ, Earles JM**.

654   **2020**. Digitally deconstructing leaves in 3D using X-ray microcomputed tomography and

655   machine learning. *Applications in Plant Sciences* **8**: e11380.

656 **Tholen D, Boom C, Noguchi K, Ueda S, Katase T, Terashima I. 2008.** The chloroplast

657   avoidance response decreases internal conductance to CO_2 diffusion in *Arabidopsis*

658   *thaliana* leaves. *Plant, Cell and Environment* **31**: 1688-1700.

659 **Tosens T, Niinemets Ü, Vislap V, Eichelmann H, Castro-Díez P. 2012.** Developmental changes

660   in mesophyll diffusion conductance and photosynthetic capacity under different light and

661   water availabilities in *Populus tremula*: how structure constrains function. *Plant, Cell &*

662   *Environment* **35:** 839-856.

663 **Tosens T, Laanisto L. 2018.** Mesophyll conductance and accurate photosynthetic carbon gain
664   calculations. *Journal of Experimental Botany* **69:** 5315-5318.

665 **Trueba S, Théroux-Rancourt G, Earles JM, Buckley TN, Love D, Johnson DM, Brodersen**
666   **C. 2021.** The 3D construction of leaves is coordinated with water use efficiency in conifers.
667   bioRxiv; doi: https://doi.org/10.1101/2021.04.23.441113

668 **Williams LE, Araujo F. 2002.** Correlations among predawn leaf, midday leaf, and midday stem
669   water potential and their correlations with other measures of soil and plant water status
670   in *Vitis vinifera* L. *Journal of the American Society for Horticultural Sciences* **127:** 448-
671   454.

672 **Willson CJ, Manos PS, Jackson RB. 2008.** Hydraulic traits are influenced by phylogenetic
673   history in the drought-resistant, invasive genus Juniperus (*Cupressaceae*). *American*
674   *Journal of Botany* **95:** 299-314.

675 **Zhong S, Yu L, Winkler JA, Tang Y, Heilman WA, Bian X. 2017.** The impact of climate change on
676   the characteristics of the frost-free season over the contiguous USA as projected by the
677   NARCCAP model ensembles. *Climate Research* **72:** 53-72.

678 **Zwieniecki MA, Brodribb TJ, Holbrook NM. 2007.** Hydraulic design of leaves: insights from
679   rehydration kinetics. *Plant, Cell and Environment*. **30:** 910-921.

680

681

682

683

684

685

686
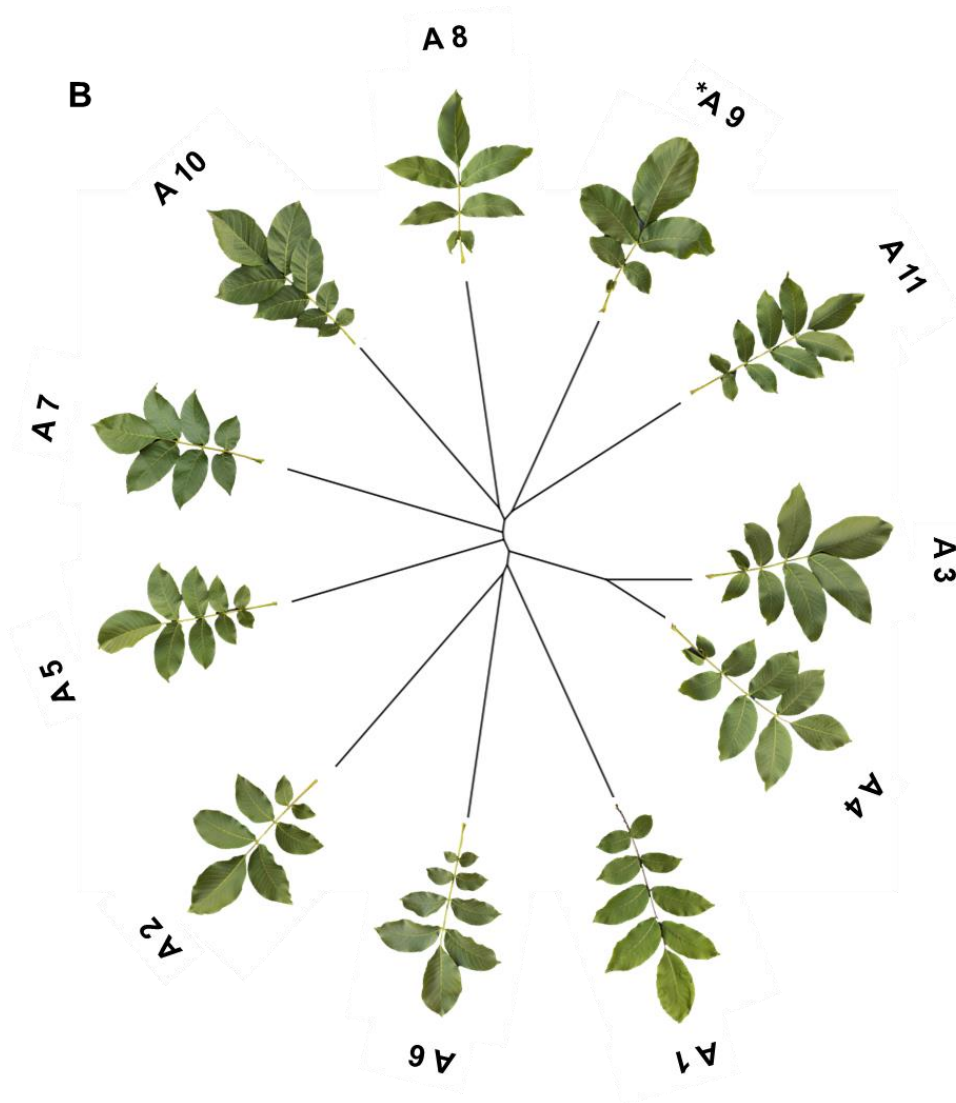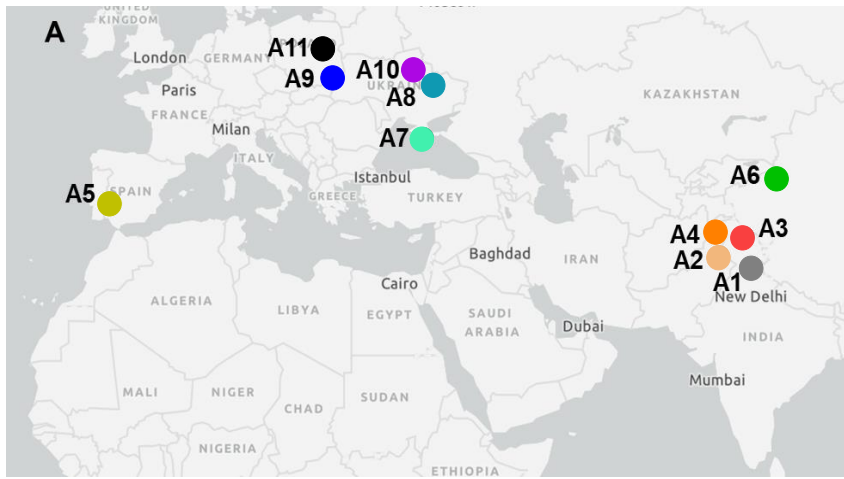
Figure 1. A. Geographic distribution map for 11 *Juglans regia* accessions. Location data were found in the USDA-ARS National Plant Germplasm System for individual accessions (GRIN). B. Unrooted neighbour-joining tree for 11 *Juglans regia* accessions. 13,320 polymorphic SNPs among these 11 trees were discovered by Illumina sequencing and used to construct NJ trees in R using the "phangorn" package. * Genotype data from C4 29, different individual but same accession as A9 (C4 28; see table S1) was used, since data for original A9 was not available.
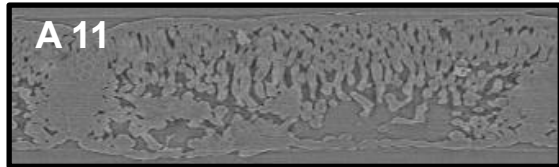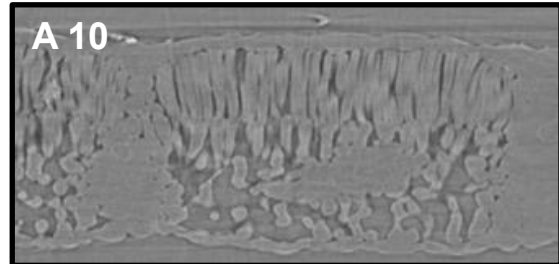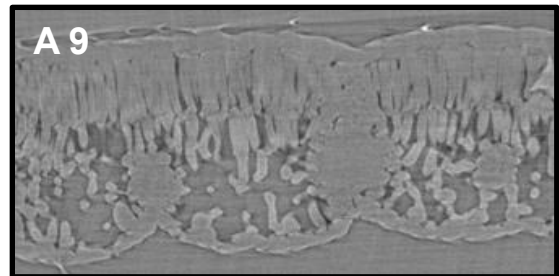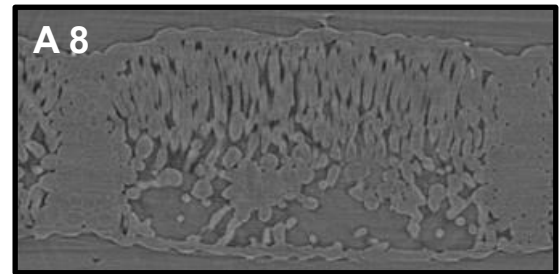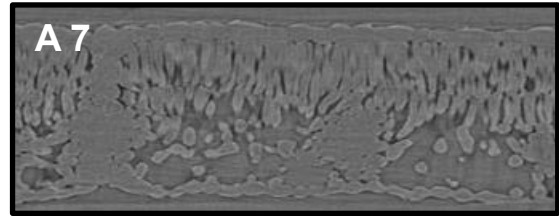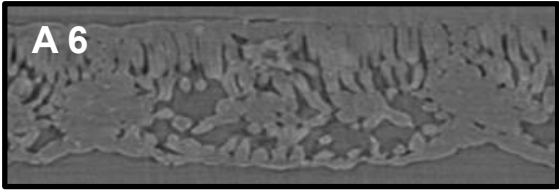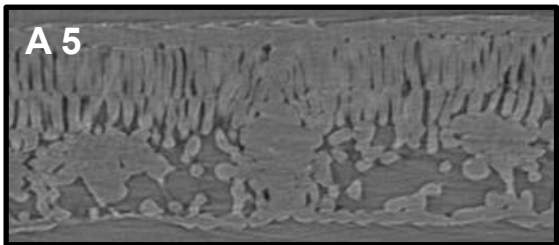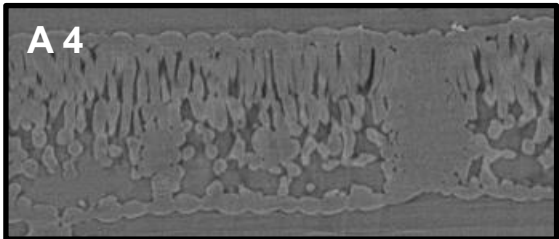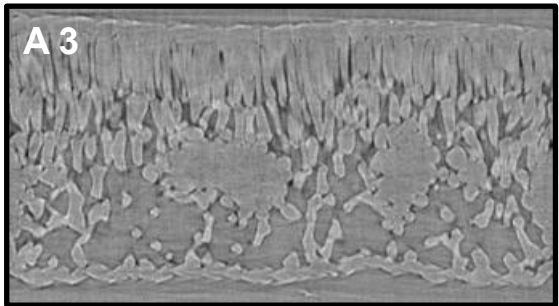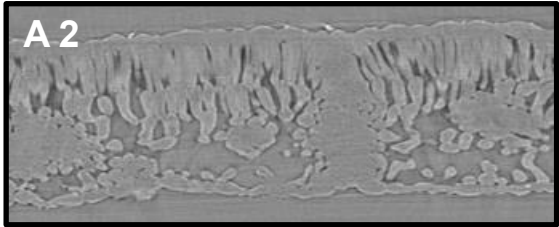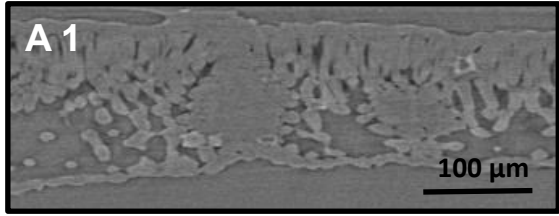
Figure 2. Leaf cross sections for 11 *J. regia* accessions under well-watered condition obtained using X-ray microcomputed tomography.
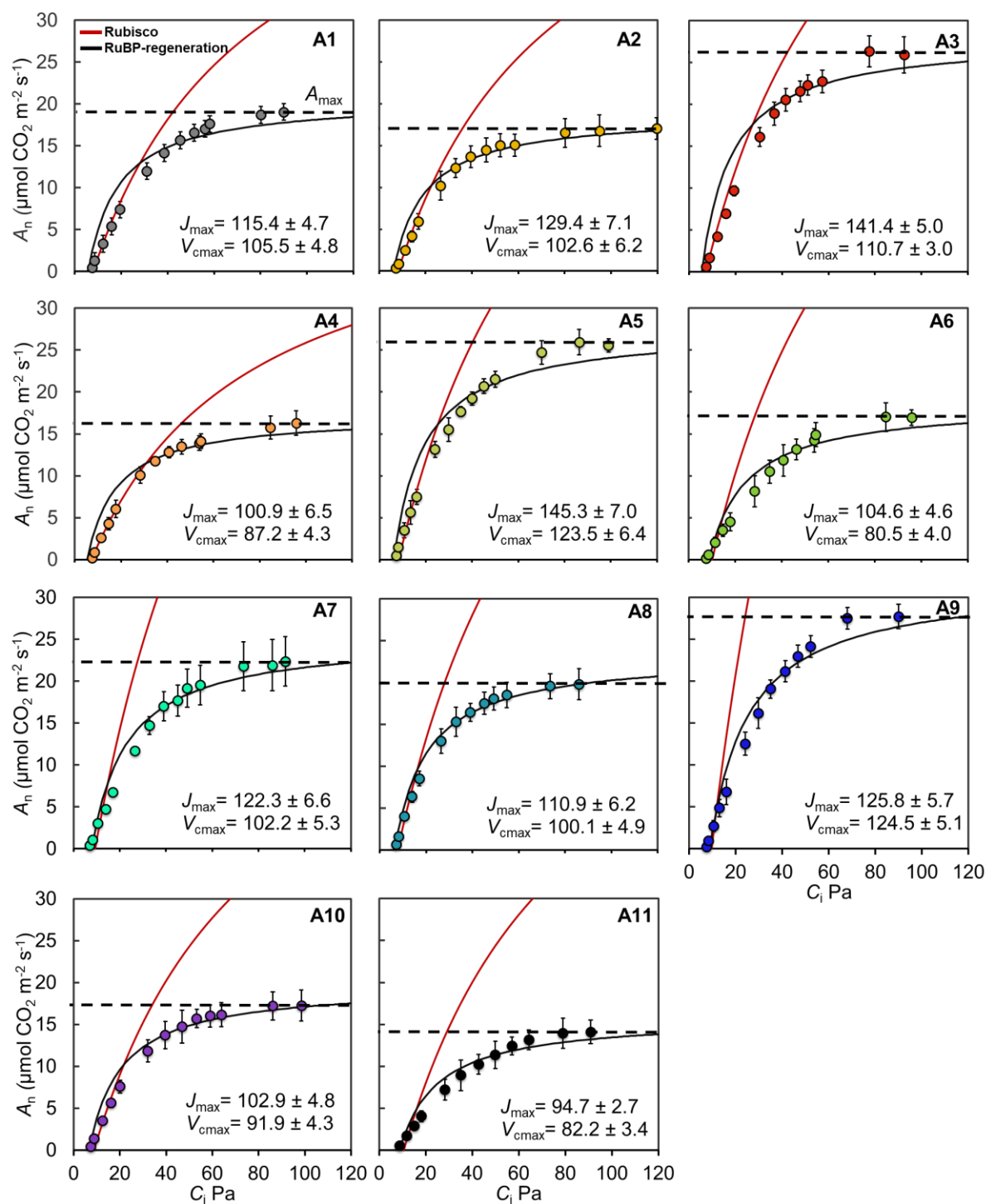
**Figure 3.** Photosynthetic CO_2 response curves were constructed using FvCB model (Sharkey 2016), averaged for five replications in 11 *J. regia* accessions under well-watered condition. Assimilation rate at saturating CO_2 (A_{max}), Rubisco and RuBP regeneration limitations are indicated for each accession. Color scheme is consistent with accession numbers presented in Figure 3 and in Table 1.

728

729
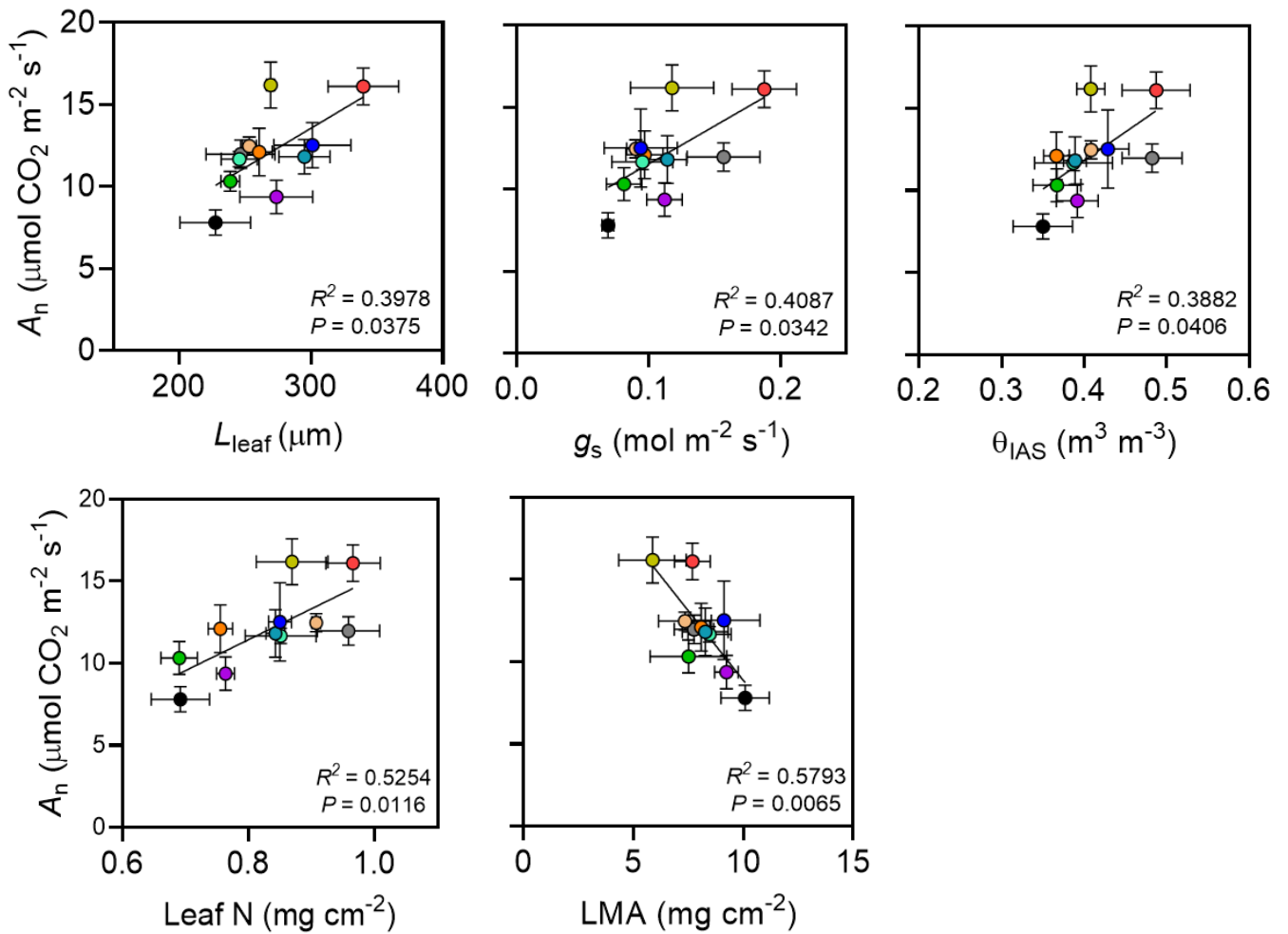
Figure 4. Net assimilation rate (A_n, µmol CO_2 m^{-2} s^{-1}) relationship with stomatal conductance (g_s, mol m^{-2} s^{-1}), mesophyll porosity (θ_{IAS}, m^3 m^{-3}), leaf thickness (L_{leaf}, µm), leaf nitrogen per unit area (leaf N, mg cm^{-2}), and leaf mass per unit area (LMA, mg cm^{-2}) in 11 *J. regia* accessions. Color scheme is consistent with accession numbers presented in Figure 3 and in Table 1.

752

753

754

755

756

34
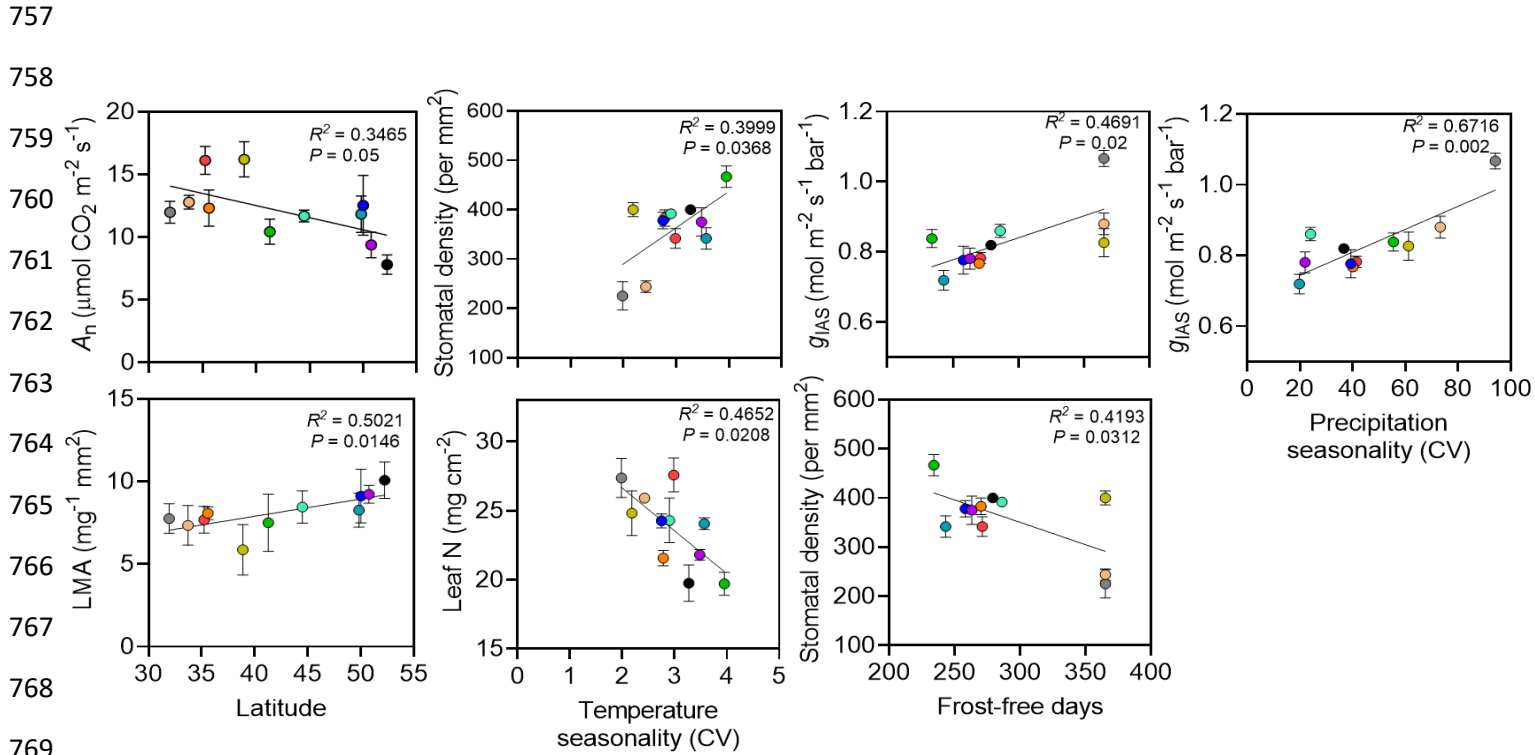
Figure 5. Relationship between net assimilation rate (A_n, μmol CO_2 m^{-2} s^{-1}), intercellular airspace conductance (g_{IAS}, mol CO_2 m^{-2} s^{-1} bar^{-1}), stomatal density (per mm^2), leaf mass per unit area (LMA, mg cm^{-2}), and leaf nitrogen per unit area (Leaf N, mg cm^{-2}) and latitude, temperature seasonality, precipitation seasonality and frost-free days in habitats for 11 *J. regia* accessions (See Fig. S4 for the full trait correlations).

Table 1. Percent change in physiological and anatomical variables under dehydration relative to the well-watered condition. Different accessions numbers are used to show significant differences under dehydration (treatment effect) from each other using mean values ($\pm$ SE) over five replications at $P < 0.002$.

Accession #	A_n	g_s	g_m	$\Psi_{leaflet}$	L_{leaf}	θ_{IAS}	g_{IAS}
A 1	-20.8 ± 0.8 (A2,3,4,5,6,8,9,10,11)	-26.0 ± 3.4 (A2,3,4,5,9,10,11)	-36.4 ± 2.4 (A2,3,4,5,6,7,8,9,10,11)	-39.8 ± 2.7 (A3,5,9)	-8.9 ± 0.8 ns	+8.4 ± 1.9 (A3)	+16.5 ± 2.2 (A2,3,6,9)
A 2	-36.2 ± 0.8 (A1,3,5,7,9,10)	-58.3 ± 0.8 (A1,4,6,7,8,9,11)	-53.4 ± 1.9 (A1,5,7)	-49.4 ± 2.3 (A3)	-11.7 ± 1.2 ns	+17.0 ± 1.9 (A8,10)	+33.3 ± 1.4 (A1,4,7,8,10,11)
A 3	-50.8 ± 1.6 (A1,2,4,6,7,8)	-66.8 ± 2.1 (A1,4,6,7,8,11)	-54.1 ± 2.6 (A1,5,7)	-66.5 ± 3.8 (A1,2,4,6,7,8,11)	-9.1 ± 0.9 ns	+21.8 ± 2.6 (A1,5,6,7,8,10,11)	+35.4 ± 2.5 (A1,4,7,8,10,11)
A 4	-36.9 ± 1.1 (A1,3,5,7,9,10)	-44.5 ± 1.1 (A1,2,3,5,6,7,8,9,10,11)	-61.1 ± 1.9 (A1,5,7,11)	-37.8 ± 3.3 (A3,5,9,10)	-7.6 ± 0.8 (A6)	+15.2 ± 1.1 (A8,10)	+21.6 ± 1.9 (A2,3)
A 5	-56.7 ± 2.2 (A1,2,4,6,7,8,10,11)	-66.7 ± 1.8 (A1,4,6,7,8)	-77.5 ± 2.5 (A1,2,3,4,6,7,8,9,10,11)	-60.9 ± 3.6 (A1,4,6,7,8)	-11.5 ± 1.2 ns	+11.3 ± 1.2 (A3)	+24.8 ± 2.1 (A7,10)
A 6	-35.6 ± 0.8 (A1,3,5,7,9,10)	-34.6 ± 0.9 (A2,3,4,5,7,9,10,11)	-60.7 ± 0.7 (A1,5,7,11)	-41.3 ± 2.6 (A3,5,9)	-13.0 ± 1.1 (A4,7,10)	+12.4 ± 2.8 (A3)	+31.2 ± 3.2 (A1,7,10,11)
A 7	-19.9 ± 1.1 (A2,3,4,5,6,8,9,10,11)	-22.3 ± 2.3 (A2,3,4,5,6,8,9,10,11)	-20.2 ± 2.6 (A1,2,3,4,5,6,8,9,10,11)	-39.7 ± 4.6 (A3,5,9)	-6.9 ± 0.9 (A6)	+10.7 ± 1.5 (A3)	+13.2 ± 1.1 (A2,3,5,6,9)
A 8	-40.7 ± 1.5 (A1,3,5,7,9)	-32.1 ± 1.6 (A2,3,4,5,7,9,10,11)	-57.8 ± 1.2 (A1,5,7)	-40.6 ± 2.8 (A3,5,9)	-9.3 ± 0.9 ns	+5.6 ± 1.2 (A2,3,4,9)	+20.8 ± 2.3 (A2,3)
A 9	-52.2 ± 1.1 (A1,2,4,6,7,8,10,11)	-71.2 ± 1.8 (A1,2,4,6,7,8)	-61.1 ± 1.4 (A1,5,7,11)	-59.5 ± 3.2 (A1,4,6,7,8)	-8.7 ± 0.9 ns	+15.5 ± 0.9 (A8,10)	+28.5 ± 3.6 (A1,7,10)
A 10	-44.9 ± 1.2 (A1,2,4,5,6,7,9,11)	-66.3 ± 1.3 (A1,4,6,7,8)	-50.2 ± 2.2 (A1,5,7)	-54.9 ± 3.1 (A4)	-7.4 ± 0.91 (A6)	+5.6 ± 1.3 (A2,3,4,9)	+12.5 ± 1.0 (A2,3,5,6)
A 11	-35.6 ± 0.8 (A1,5,7,9,10)	-75.8 ± 4.2 (A1,2,3,4,6,7,8)	-49.4 ± 3.3 (A1,4,5,6,7,9)	-46.5 ± 1.8 (A3)	-8.3 ± 0.9 ns	+12.1 ± 2.3 (A3)	+19.4 ± 1.8 (A2,3,6)
P value	< 0.002	< 0.002	< 0.002	< 0.002	< 0.002	< 0.002	< 0.002

A_n, net assimilation rate (μmol CO_2 m^{-2} s^{-1}); g_s, stomatal conductance (mol m^{-2} s^{-1}); g_m, mesophyll conductance (mol CO_2 m^{-2} s^{-1}); $\Psi_{leaflet}$, leaflet water potential (MPa); L_{leaf}, leaf thickness (μm); θ_{IAS}, mesophyll porosity (m^3 m^{-3}), g_{IAS}, intercellular airspace conductance (mol m^{-2} s^{-1} bar^{-1}).

Table 2. Pearson correlation coefficients between the absolute values of the physiological and anatomical variables and climatic data for 11 *J. regia* accessions under dehydration treatment. Bold indicates significance at $P < 0.05$ and * indicates significance after Bonferroni corrections ($P < 0.0025$).

|	Latitude	Temperature seasonality (CV)	Precipitation seasonality (CV)	Frost-free days
A_n	**-0.728***	-0.541	0.447	0.553
g_m	**-0.675**	-0.475	0.311	0.538
θ_{IAS}	**-0.603**	-0.474	0.483	0.420
g_{IAS}	**-0.712***	-0.435	**0.856***	0.582
Leaf N	**-0.603**	-0.083	0.372	0.01

Supporting Information

Table S1. Geographic data for origins of 11 *J. regia* accessions collected at the US National Germplasm Repository located at the Wolfskill Experimental Orchard.

| Accession #	Latitude (°N)	Longitude (E)	Elevation (m)	Plant Name	Accession name in Wolfskill repository	Location in Wolfskill	Precipitation seasonality	Temperature seasonality	Frost-free days
1	31.95	77.10	1199	Lang Thacha	DJUG0486.	C 11 14	84.13	1.98	365
2	33.71	73.08	562	Ahkrot	DJUG0275.1	C 3 28	69.25	2.42	365
3	35.23	75.96	2637	880638	DJUG0274.4	C 3 27	49.42	2.98	295
4	35.60	72.65	4089	880432	DJUG0260.4	C 2 14	40.04	2.78	280
5	38.87	- 6.97	170	Badajoz	DJUG0420.	C 4 36	66.20	2.18	365
6	41.27	80.23	1131	Aksu 81	DJUG0377.8	C 8 32	55.44	3.95	234
7	44.49	34.16	10	Op Sdlg/paperovii	DJUG0188.1	A 2 34	21.96	2.90	286
8	49.83	35.61	121	DJUG 566	DJUG0566.4	C 16 8	29.74	3.56	253
9	50.01	22.22	238	Nn 88 Godyn	DJUG0413.	C 4 28	39.33	2.75	258
10	50.75	33.50	111	DJUG 606	DJUG0606	C 20 2	21.93	3.48	253
11	52.22	21.01	114	R 8/6	DJUG0411.	C 13 38	31.64	3.27	269
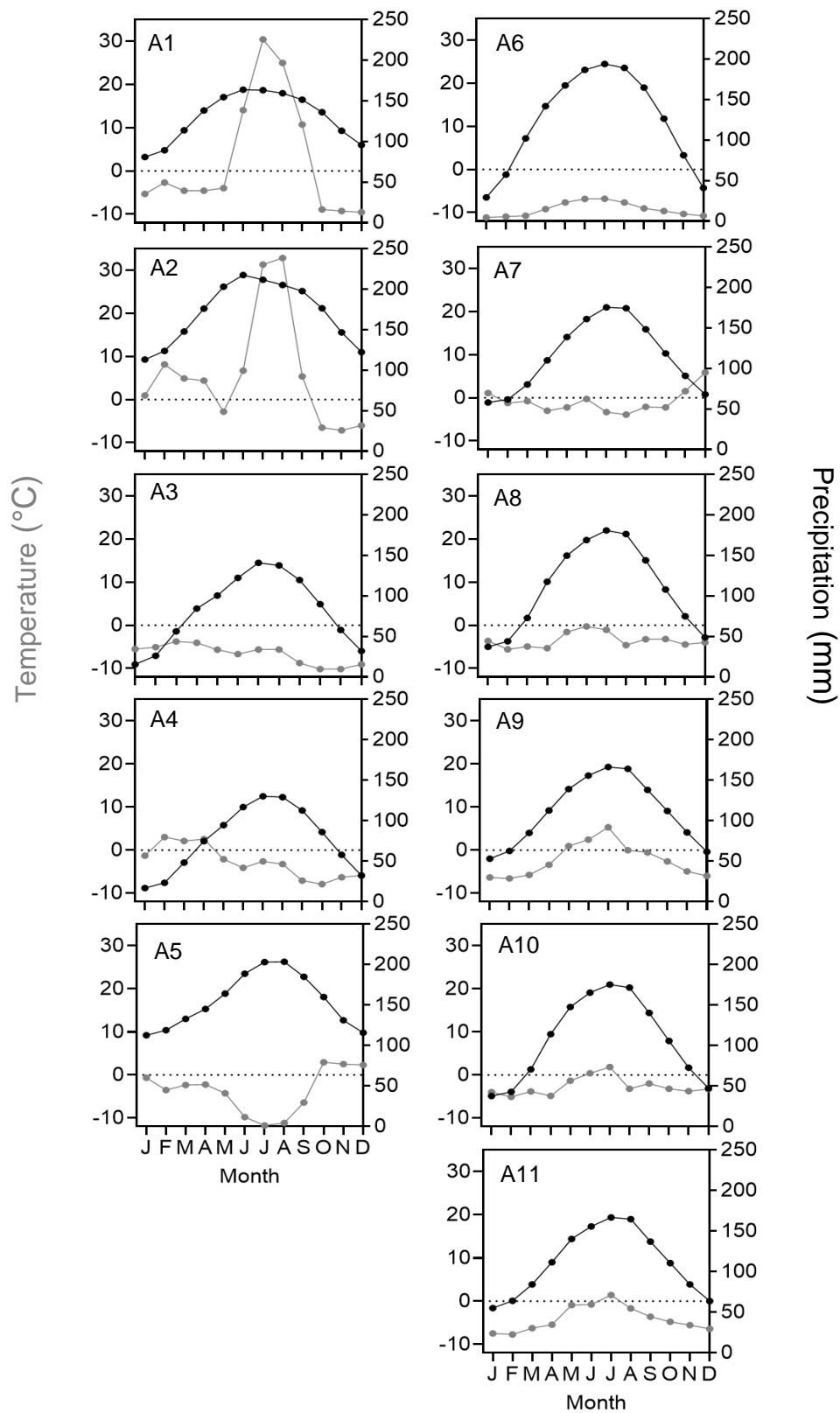
Figure S1. Walter-Lieth climate diagrams for 11 *J. regia* habitats. The diagrams present average monthly temperature (grey) and annual precipitation (black). Sources: https://climatecharts.net/, https://climateknowledgeportal.worldbank.org/download-data. Latitude is positively correlated with the temperature seasonality ($P = 0.049$), and negatively related to precipitation seasonality ($P = 0.004$), and frost-free days ($P = 0.016$). As expected, low-latitude habitats showed more frost-free days and higher variability in precipitation seasonality (Zhong *et al.* 2017; Marelle *et al.* 2018; Liu *et al.* 2018).

39
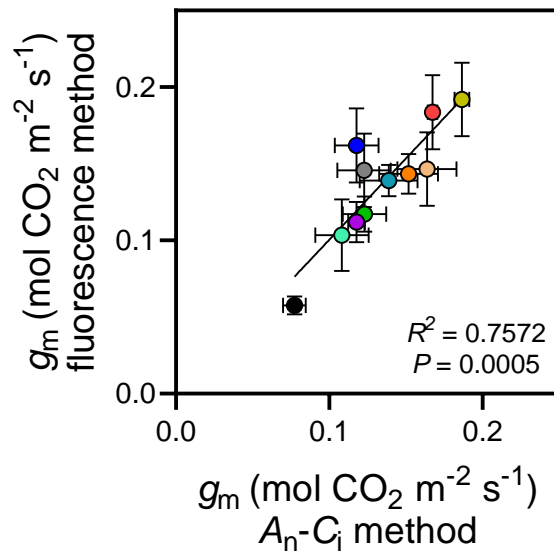
Figure S2. Correlation between mesophyll conductance (g_m, mol CO_2 m^{-2} s^{-1}) obtained from chlorophyll fluorescence and A_n-C_i curve methods for five reps (± SE) for each of 11 *J. regia* accessions under well-watered treatment.

A 1

A11

High porosity
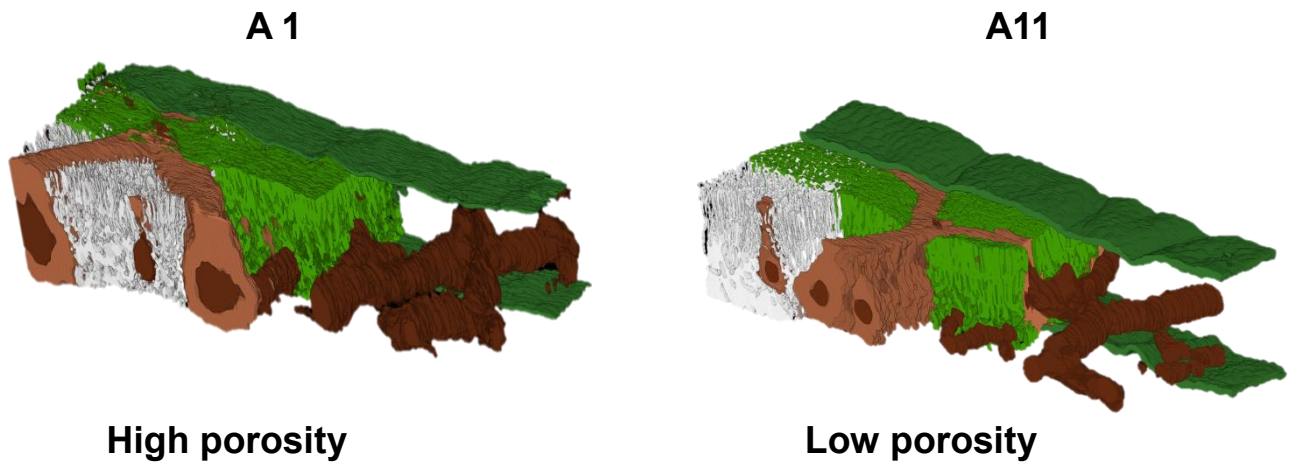
Low porosity

Figure S3. 3D projection of whole leaf for A1 and A11, high and low mesophyll porosity accessions, respectively.
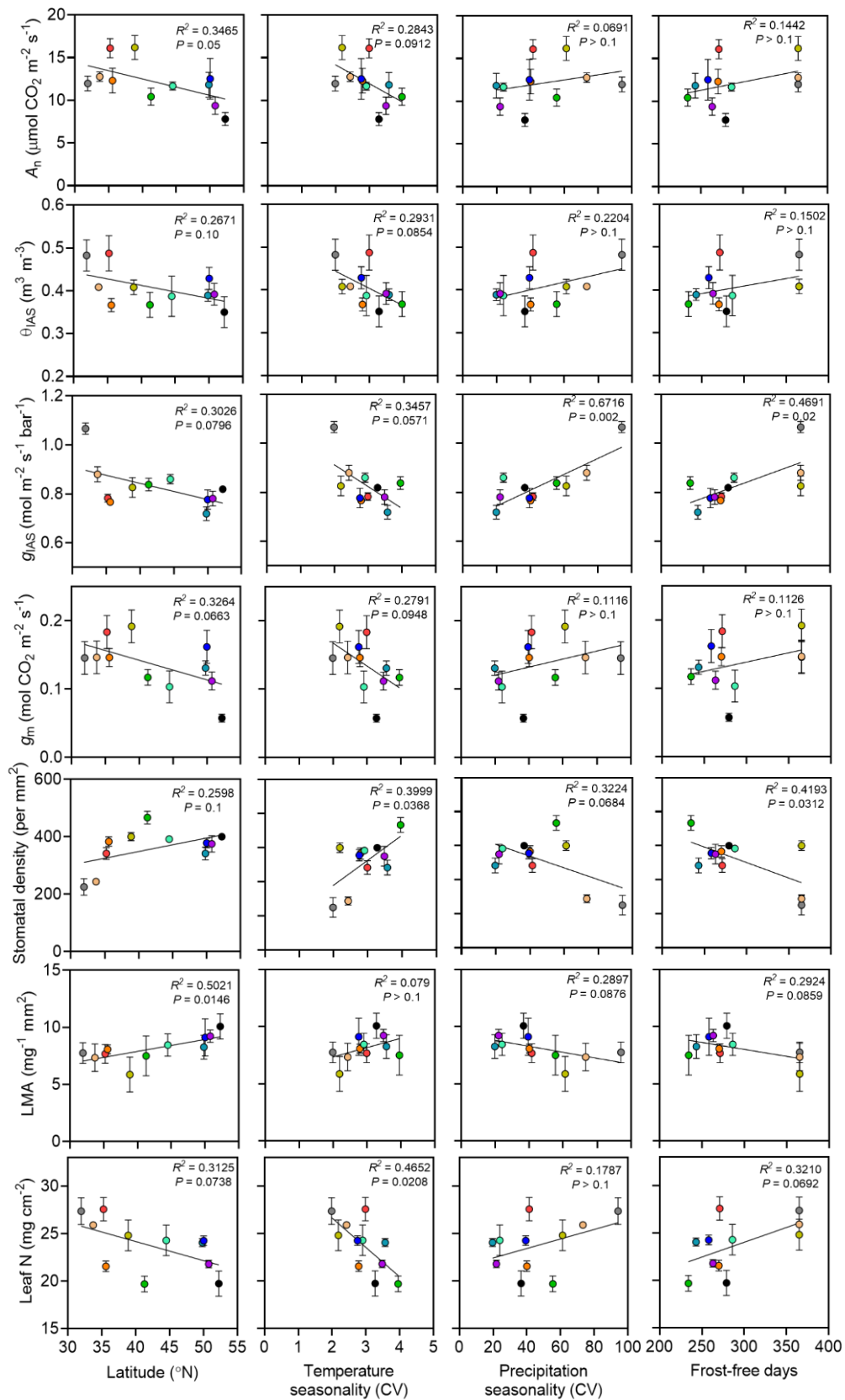
Figure S4. Relationship between net assimilation rate (A_n, μmol CO_2 m^{-2} s^{-1}), mesophyll porosity (θ_{IAS}, m^3 m^{-3}), intercellular airspace conductance (g_{IAS}, mol CO_2 m^{-2} s^{-1} bar^{-1}), mesophyll conductance (g_m, mol CO_2 m^{-2} s^{-1}), stomatal density (per mm^2), leaf mass per unit area (LMA, mg cm^{-2}), and leaf nitrogen per unit area (Leaf N, mg cm^{-2}) and latitude, temperature seasonality, precipitation seasonality and frost-free days in habitats for 11 *J. regia* accessions.
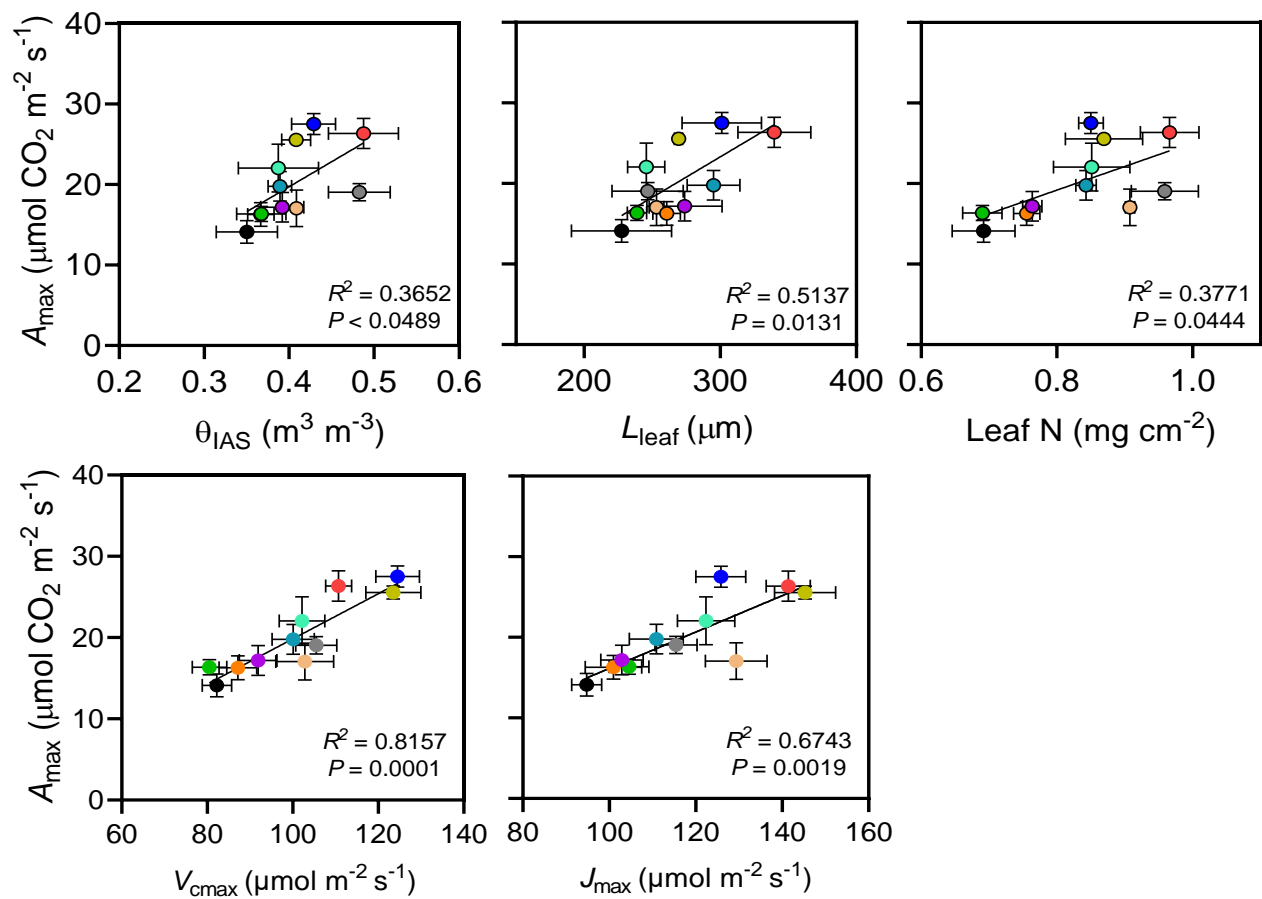
Figure S5. Assimilation rate at saturating CO_2 (A_{max}, µmol CO_2 m^{-2} s^{-1}) relationship with mesophyll porosity (θ_{IAS}, m^3 m^{-3}), leaf thickness (L_{leaf}, µm), and leaf nitrogen per unit area (Leaf N, mg cm^{-2}), maximum carboxylation rate (V_{cmax}) and maximum electron transport rate (J_{max}) in 11 *J. regia* accessions.
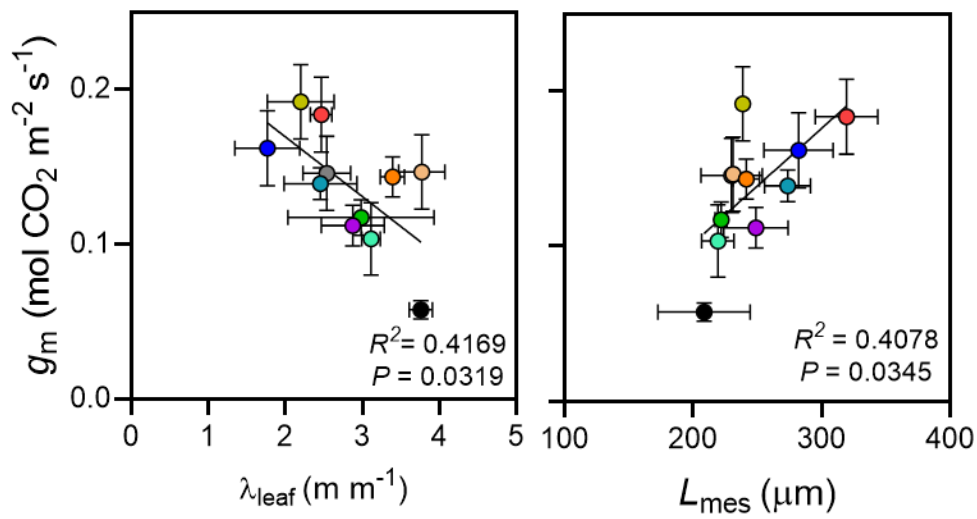
Figure S6. Mesophyll conductance (g_m, mol CO_2 m^{-2} s^{-1}) relationship with lateral path lengthening (λ_{leaf}, m m^{-1}), mesophyll thickness (L_{mes}, μm) in 11 *J. regia* accessions under well-watered condition.

Table S2. Absolute values for physiological and anatomical variables under dehydration treatment. Different accessions numbers are used to show significant differences from each other using mean values (± SE) over five replications at $P < 0.002$.

Accession #	A_n	g_s	g_m	$\Psi_{leaflet}$	L_{leaf}	θ_{IAS}	g_{IAS}
A 1	9.49 ± 0.69 (A9,10,11)	0.11 ± 0.04 (A11)	0.09 ± 0.01 (A5,11)	-1.05 ± 0.05 (A2,4,5,9,10,11)	224.50 ± 6.93 (A3)	0.53 ± 0.08 ns	1.28 ± 0.23 ns
A 2	7.96 ± 1.02	0.04 ± 0.01 ns	0.07 ± 0.02 ns	-1.40 ± 0.03 (A1,6)	223.35 ± 7.59 (A3)	0.49 ± 0.06 ns	1.32 ± 0.26 ns
A 3	7.92 ± 1.16 ns	0.06 ± 0.02 ns	0.08 ± 0.03 ns	-1.14 ± 0.13 (A5,9,10)	308.75 ± 15.28 (A1,2,4,5,6,7,10,11)	0.62 ± 0.08 ns	1.21 ± 0.12 (A11)
A 4	7.63 ± 0.78 ns	0.05 ± 0.01 ns	0.06 ± 0.01 ns	-1.42 ± 0.04 (A1,6,8)	240.68 ± 10.27 (A3)	0.43 ± 0.01 ns	0.98 ± 0.15 ns
A 5	7.00 ± 1.40 ns	0.04 ± 0.01 ns	0.04 ± 0.01 (A1)	-1.63 ± 0.04 (A1,3,6,7,8)	238.29 ± 12.68 (A3)	0.46 ± 0.01 ns	1.10 ± 0.02 ns
A 6	6.64 ± 0.61 ns	0.05 ± 0.01 ns	0.05 ± 0.01 ns	-0.97 ± 0.04 (A2,4,5,9)	207.72 ± 4.66 (A3,8,9)	0.42 ± 0.03 ns	1.22 ± 0.26 ns
A 7	9.35 ± 1.67 ns	0.07 ± 0.02 ns	0.08 ± 0.03 ns	-1.31 ± 0.02 (A5,7,9,10,11)	228.67 ± 12.57 (A3)	0.43 ± 0.02 ns	0.99 ± 0.05 ns
A 8	7.01 ± 0.94 ns	0.08 ± 0.02 ns	0.06 ± 0.01 ns	-1.11 ± 0.06 (A4,5,9,10,11)	267.81 ± 8.84 (A11)	0.41 ± 0.01 ns	0.91 ± 0.19 ns
A 9	5.98 ± 0.84 (A1)	0.03 ± 0.01 ns	0.06 ± 0.01 ns	-1.50 ± 0.09 (A1,3,6,8)	274.79 ± 6.87 (A11)	0.51 ± 0.04 ns	1.09 ± 0.12 ns
A 10	5.16 ± 1.34 (A1)	0.04 ± 0.01 ns	0.06 ± 0.01 ns	-1.48 ± 0.03 (A1,3,8)	253.49 ± 15.09 (A3)	0.42 ± 0.01 ns	0.89 ± 0.09 ns
A 11	5.03 ± 0.81 (A1)	0.02 ± 0.01 (A1)	0.03 ± 0.01 (A1)	-1.42 ± 0.06 (A1,8)	208.50 ± 10.79 (A3)	0.39 ± 0.02 ns	1.04 ± 0.24 (A3)
P value	< 0.002	< 0.002	< 0.002	< 0.002	< 0.002	< 0.002	< 0.002